AD-A204 740

REPORT DOCUMENTATION PAGE

DTIC ELECTE FEB 17 1989 S D

DTIC FILE COPY

1a. Unclassified	1b. RESTRICTIVE MARKINGS
2a. SECURITY CLASSIFICATION AUTHORITY	3. DISTRIBUTION / AVAILABILITY OF REPORT: Approved for Pulbic Release; Distribution unlimited
2b. DECLASSIFICATION / DOWNGRADING SCHEDULE	
4. PERFORMING ORGANIZATION REPORT NUMBER(S)	5. MONITORING ORGANIZATION REPORT NUMBER(S): AFOSR-TR- 89-0134
6a. NAME OF PERFORMING ORGANIZATION: JAYCOR	6b. OFFICE SYMBOL (If applicable)
7a. NAME OF MONITORING ORGANIZATION: AFOSR/NP	
6c. ADDRESS (City, State, and ZIP Code): 11011 Torreyana Road, PO BOX 85154, San Diego CA 92138-9259	7b. ADDRESS (City, State, and ZIP Code): Building 410, Bolling AFB DC 20332-6448
8a. NAME OF FUNDING / SPONSORING ORGANIZATION: Same as 7a	8b. OFFICE SYMBOL (If applicable)
9. PROCUREMENT INSTRUMENT IDENTIFICATION NUMBER: F49620-86-C-0068	
8c. ADDRESS (City, State, and ZIP Code): Same as 7b	10. SOURCE OF FUNDING NUMBERS

PROGRAM ELEMENT NO.	PROJECT NO.	TASK NO.	WORK UNIT ACCESSION NO.
61102F	2301	A8	

11. TITLE (Include Security Classification)

"THEORY RELATED TO A MM WAVE SOURCE EXPERIMENT"

12. PERSONAL AUTHOR(S): Dr M Rosenberg

13a. TYPE OF REPORT	13b. TIME COVERED	14. DATE OF REPORT (Year, Month, Day)	15. PAGE COUNT
Final	FROM 1 May 86 TO 30 Sep 88	October 1988	83

16. SUPPLEMENTARY NOTATION

17. COSATI CODES			18. SUBJECT TERMS (Continue on reverse if necessary and identify by block number)
FIELD	GROUP	SUB-GROUP	

19. ABSTRACT (Continue on reverse if necessary and identify by block number)

Much progress was made in characterizing the principal plasma physics phenomena involved in the plasma 3 wave mixing scheme under experimental investigation by Dr Bob Schumacher of Hughes Research Labs. Bennett pinching was found to be extremely important in focussing the counterstreaming electron beams in the device. The ion modulation instability was identified as the crucial remaining issue to be studied for improving the signal purity of this millimeter wave source.

20. DISTRIBUTION / AVAILABILITY OF ABSTRACT	21. ABSTRACT SECURITY CLASSIFICATION
☒ UNCLASSIFIED/UNLIMITED ☒ SAME AS RPT ☐ DTIC USERS	Unclassified

22a. NAME OF RESPONSIBLE INDIVIDUAL	22b. TELEPHONE (Include Area Code)	22c. OFFICE SYMBOL
Dr Robert J. Barker	202/767-5011	NP

DD FORM 1473, 84 MAR — 83 APR edition may be used until exhausted. All other editions are obsolete.

SECURITY CLASSIFICATION OF THIS PAGE

UNCLASSIFIED

J530-88-664/2473

FINAL REPORT ON

AFOSR-TR- 89-0134

THEORY RELATED TO A

MM WAVE SOURCE EXPERIMENT

Covering 1 May 86 thru 30 Sept 88

Prepared by

JAYCOR
11011 Torreyana Road
San Diego, CA 92138-9259
(619) 453-6580

Prepared for

AFOSR
Bolling Air Force Base
Washington, D.C.

under

Contract No. F49620-86-C-0068

October 1988

89 2 16 084

JAYCOR

QUALITY INSPECTED 4

August 9, 1988

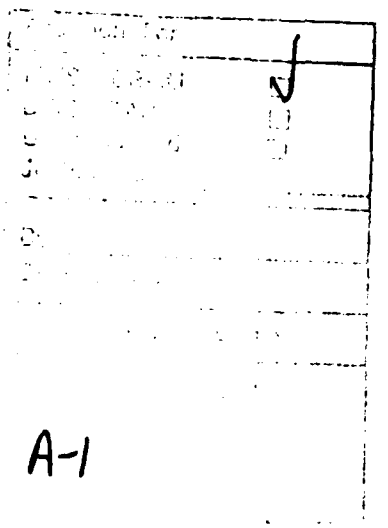

AFSOR
Directorate of Physical and
Geophysical Sciences
Building 410
Bolling Air Force Base
Washington, DC 20332-6448

Attention: Dr. Robert Barker

Subject: Contract No. F49620-86-C-0068
JAYCOR Project No. 2472

A-1

Dear Dr. Barker:

Dr. Dave Sargis has forwarded to me the file and responsibilities relating to the referenced contract. In response to what I understand is your request to Dave, I have accordingly enclosed a single copy of the three reports which the file indicates have been developed for the contract, and I list the references to the two oral presentations which the file indicates have been presented. I also provide a short summary of the work which has been completed. I close this correspondence with the suggestion that electromagnetic particle simulations, which we are fully capable of undertaking, could be advantageously applied to the investigation of the HRL millimeter-wave source.

The three reports, which have been completed under the referenced contract are:

1. M. Rosenberg and N. A. Krall, "Theory Related to a MM Wave Source Experiment," Rep. J530-87-703/2472, JAYCOR, San Diego, CA (1987).

2. M. Rosenberg and N. A. Krall, "Theory Related to a MM Wave Source Experiment," Rep. J530-87-718/2472, JAYCOR, San Diego, CA (1987).

3. M. Rosenberg and N. A. Krall, "Theory of a MM-Wave Source Experiment," Rep. J530-88-726/2472, JAYCOR, San Diego, CA (1988).

The references to the two oral presentations (at APS Plasma Physics Meetings) are:

1. M. Rosenberg and N. A. Krall, "Phenomenology of MM Wave Plasma Source Experiments," Bull. Am. Phys. Soc. 31, 1602 (1986).

2. M. Rosenberg and N. A. Krall, "Theory of a MM-Wave Plasma Source Experiment," Bull. Am. Phys. Soc. 32, 1885 (1987).

11011 Torreyana Road — Post Office Box 85154 • San Diego, California 92138-9259 • (619) 453-6580

The referenced contract has provided theoretical support for the HRL (Hughes Research Laboratories) experiment which is intended to demonstrate the production of millimeter-wavelength radiation by the three-wave mixing concomitant with the interaction of counterstreaming electron beams in a plasma-filled waveguide/cavity. The specific objectives of the research has been to investigate 1) beam dynamics, 2) linear beam-plasma interactions, 3) nonlinear beam-plasma interactions, 4) radiative mechanisms, and 5) mechanisms for the temporal modulation of radiation.

The results of the research can be summarized as six major points. 1) The beam dynamics may be controlled by the magnetic self-focusing and ionization; however, an inconsistency may be evident insofar as the required length for magnetic focusing appears to be larger than the length of the device. 2) The dominant beam-plasma interaction is Cerenkov excitation of electron plasma waves with a discrete spectrum. 3) The unstable electron-plasma waves grow to an amplitude determined by beam saturation on the fast electron time scale. 4) The scaling of the radiative electromagnetic power is consistent with weak turbulence estimates. 5) The saturated electron-plasma waves can have sufficient amplitude to excite the modulational instability. 6) The temporal modulation of radiation, observed in the experiment on the ion time scale, may be a consequence of strong turbulence effects.

The capabilities of JAYCOR's Electromagnetic Applications Division are summarized in a separate enclosure. In particular, the capability to do electromagnetic particle simulations could be advantageously applied to the development of the HRL millimeter-wave source. The particle simulations are particularly applicable to the understanding and interpretation of nonlinear processes which are often difficult to assess from a purely theoretical standpoint, and they can be used for comparison with the nonlinear models, developed under the referenced contract, for an initially homogeneous plasma.

I hope this letter and the enclosures benefit you; however, if any additional requirements remain, I can be reached directly at (619) 535-3168. I tentatively have plans to be on the East Coast in October, and I would appreciate at that time to have the opportunity to set up an appointment with you in order to discuss our capabilities relative to your programs.

Sincerely,

J. L. Sperling

J. L. Sperling, Manager
Electromagnetic Applications Division

JLS/heh

Enclosures

ELECTROMAGNETIC APPLICATIONS

The Electromagnetic Applications Division, a component of JAYCOR's System Survivability and Technology Applications Group in San Diego, uses its background in electromagnetic theory and numerical simulation to address a complex set of practical problems, ranging from theoretical, numerical, and experimental investigations of laboratory and space plasmas to radar jamming and algorithm development for systems codes.

The resources of the Electromagnetic Applications Division include expertise in the theory of plasma stability, transport, and heating, along with off-the-shelf numerical models applicable to mirror machines, reversed field configurations, tokamaks, imploding liners, magnetic solenoids, z-pinches, plasma switches, and other plasma devices. The numerical models include fluid codes, particle-pusher codes, hybrid codes, and dispersion-relation solvers. Areas of application include microinstability and macroinstability phenomenology, prediction of the behavior of plasma devices, explanation of the results of space and laboratory plasma experiments, calculation of wave absorption and propagation in plasmas, and calculation of energy loss rates from magnetically confined plasmas. Other applications include tomography, ion-cyclotron emission from plasmas, and the analysis of microwave-driven neutralizers and negative-ion sources for intense neutral beams.

One ongoing program has been the creation and implementation of numerical algorithms for the development of communication systems, radars, and sensors which are robust to the deleterious scintillation and clutter associated with high-altitude plasma structures. The work has involved the discernment of various plasma transport processes, such as viscosity, as being key to the phenomenon of "frozen" striations. New and innovative techniques have been developed to numerically analyze structure

evolution in three dimensions, and an innovative experiment has successfully simulated the formation of high-altitude striations in the laboratory.

The Division has the in-house capability to predict disturbed high-altitude environments and the effect of the environments upon communication links and radars. The Division's expertise, in disturbed high-altitude environments, has been used to solve additional problems significant to National security. For example, the penetration of directed energy weapons has been investigated through disturbed environments determined by numerical simulations. Personnel have also contributed to the writing of an EM-1 manual commissioned by the Defense Nuclear Agency.

The expertise of the Electromagnetic Applications Division has been used to analyze the formation of free-electron populations during the high-hypersonic flight of reentry vehicles and the generation of electricity based upon magnetohydrodynamic principles. One aspect of this work has been the application of radar equations to determine the potential for disrupting the operation of ground-based radars.

Important contributions, to the development of high-voltage plasma-opening switches, have been made through the successful application of fluid and hybrid simulations which have characterized parametric ranges for successful operation. This work is directly relevant to the development of the Particle Beam Fusion Accelerator II (PBFA II) at Sandia National Laboratories.

In all areas, the Electromagnetic Applications Division has broad analytic, numerical, and experimental capabilities in applied electromagnetism and continues to be committed to the application of its expertise to the highly responsive solution of problems vital to government and industry.

CONTACT:

Dr. Jacob L. Sperling
(619) 453-6580 or
(619) 535-3168 (Direct)

TABLE OF CONTENTS

Section			Page
1	INTRODUCTION		1
2	EXECUTIVE SUMMARY		2
3	STANDARD CASE PARAMETERS		5
4	SUMMARY AND APPLICATIONS OF LITERATURE		8
	4.1	MAGNETIC SELF FOCUSING	8
		4.1.1 Summary of Literature	8
		4.1.1.1 Bennett Pinch Condition	8
		4.1.1.2 Charge Neutralization	8
		4.1.1.3 Current Neutralization	9
		4.1.1.4 Bennett Equilibrium	9
		4.1.2 Application to mm Wave Experiment	10
		4.1.2.1 Introduction	10
		4.1.2.2 Beams are Charge and Current Neutralized	12
		4.1.2.3 Beam Subject to Bennett Pinch	14
		4.1.2.4 Bennett Equilibrium	15
		4.1.2.5 Implications	15
		4.1.2.6 Work to be Done	15
	4.2	BEAM-PLASMA AND TWO-STREAM INSTABILITIES	16
		4.2.1 Summary of Literature	16
		4.2.1.1 Introduction	16
		4.2.1.2 Beam-Plasma Instabilities in a Plasma-Filled Waveguide	16
		4.2.2 Application to mm Wave Experiment	27
		4.2.2.1 Introduction	27
		4.2.2.2 Beam in Plasma-Filled Waveguide: Beam Radius = Guide Radius	27
		4.2.2.3 Thin Beam: Axisymmetric Modes	28
		4.2.2.4 Thermal Effects on Beam-Plasma Instability: Limits on $k_\perp$	29
		4.2.2.5 Quantization of k_z	29
		4.2.2.6 Work to be Done	30

TABLE OF CONTENTS (Continued)

Section			Page
4.3	BEAM STABILIZATION		33
	4.3.1	Summary of Literature	33
		4.3.1.1 Introduction	33
		4.3.1.2 Beam Trapping	33
		4.3.1.3 Nonlinear Stabilization	34
		4.3.1.4 Quasilinear Stabilization	42
	4.3.2	Application to mm Wave Experiment	43
		4.3.2.1 Beam Trapping and Quasilinear Stabilization	43
		4.3.2.2 Nonlinear Stabilization	45
		4.3.2.3 Time Scale of Modulation of the Radiation	50
		4.3.2.4 Work to be Done	50
4.4	RADIATION MECHANISMS		52
	4.4.1	Summary of Literature	52
		4.4.1.1 Introduction	52
		4.4.1.2 Emission Mechanisms for $2\omega_{pe}$ Radiation	53
		4.4.1.3 Emission Mechanisms for ω_{pe} Radiation	56
	4.4.2	Application to mm Wave Experiment	59
		4.4.2.1 Emission Mechanisms for $2\omega_{pe}$ Radiation	59
		4.4.2.2 Emission Mechanisms for ω_{pe} Radiation	64
		4.4.2.3 Work to be Done	66
4.5	OTHER EXPERIMENTS		67
	4.5.1	Experiment A	67
		4.5.1.1 Summary of Experimental Results	67
		4.5.1.2 Relation to mm Wave Experiment	72
	4.5.2	Experiment B	73
		4.5.2.1 Summary of Experimental Results	73
		4.5.2.2 Relation to mm Wave Experiment	74
	4.5.3	Experiment C	75
		4.5.3.1 Summary of Experimental Results	75

TABLE OF CONTENTS (Continued)

Section		Page
4.5.4	Experiment D	75
4.5.4.1	Summary of Experimental Results	75
4.5.4.2	Relation to mm Wave Experiment	76
4.5.5	Experiment E	76
4.5.5.1	Summary of Experimental Results	76
4.5.5.2	Relation to mm Wave Experiment	77
4.5.6	Experiment F	77
4.5.6.1	Summary of Experimental Results	77
4.5.6.2	Relation to mm Wave Experiment	79
5	REFERENCES	80

1. INTRODUCTION

The beam-plasma experiment conducted by R. W. Schumacher and J. Santoru at Hughes Research Laboratories appears to be a promising technique for the production of high power mm wavelength radiation. This approach uses two counterstreaming electron beams in a plasma-filled waveguide. Each beam excites unstable waves at the plasma frequency. The nonlinear coupling of these beam excited waves produces an electromagnetic waveguide mode at twice the plasma frequency.

This report provides a basis for theoretical support of this experiment, which will often be referred to as the mm wave experiment in this report. It includes (1) a summary and analysis of state-of-the-art theories and experiments which are relevant to this experiment, and (2) application of this material to explain experimental observations.

The report is arranged in the following way. An executive summary is provided in Section 2. This summarizes the main points of the relevant literature, and the main experimental observations that can be understood through the application of elements of this literature. A set of standard case parameters are given in Section 3. These parameters are representative of experimental conditions, and will be used in the following application sections. The largest part of the report, Section 4, deals with a summary and application of the literature. It is divided into four main physics topics--beam focusing, beam-plasma instability, beam stabilization, and radiation mechanisms--and a section on related experiments. Within each topic, the relevant literature is first summarized. Then, elements of existing theory are used to explain various experimental observations. In the section on related experiments, the relation between this mm wave experiment and other relevant experiments is elucidated.

2. EXECUTIVE SUMMARY

Application of the results of a literature search has yielded insights into the physics of Schumacher and Santoru's mm wave production experiment. In some areas, there is remarkable agreement between theoretical estimates and experimental results.

MAIN POINTS

1. The beam dynamics can be understood in terms of the Bennett pinch and the Bennett equilibrium. There is much literature on charge neutralization of a beam (pgs. 8-9), beam current neutralization (pg. 9), the Bennett pinch (pg. 8), and Bennett equilibria (pgs. 9-10).

Estimates show that each beam in this mm wave experiment is charge neutralized, and return currents are negligible (pgs. 12-14). When the beam current is above the Bennett threshhold, it should pinch. The beam should be constricted, or focused, by it's self generated magnetic field, whose energy exceeds the beam's perpendicular thermal energy (pg. 14). The experimentally determined profile of the focused beam can be fit with a Bennett equilibrium profile. The theoretical values for the beam profile radius are in good agreement with the experimentally measured ones (pg. 15).

2. The dominant beam-plasma instability is the Cerenkov instability of each beam. The literature treats a plasma-filled waveguide, for which the beam radius is the same as the guide radius (pgs. 16-19), the beam radius is much less than the guide radius (pg. 19), or the beam radius is arbitrary (pgs. 19-25). There is also literature on two counterstreaming electron beams in an unbounded plasma (pgs. 25-27).

Calculation indicates that the dominant beam-plasma instability in the mm wave experiment is the Cerenkov beam-plasma instability of each beam, which produces waves at the plasma frequency ω_{pe}. The axial wavevector k_z satisfies the Cerenkov condition $\omega_{pe} \sim k_z v_b$, with v_b the beam velocity (pg. 27). When the beam is thin, and concentric with the guide, the modes excited are axisymmetric TM_{0np} modes (pg. 28). The waveguide wall does not have a stabilizing effect when the beam edge is more than a couple of collisionless

skin depths distant, which is the case in this experiment (pg. 28). The effect of the radial wall is to quantize $k_\perp$; the perpendicular wavevectors are constrained to be discrete because of boundary conditions involving Bessel functions (pgs. 27-28).

3. The stabilization of beam-plasma instabilities can be understood within the context of beam trapping and nonlinear parametric instabilities. Most of the literature on beam saturation deals with unbounded plasmas. (However, quasilinear beam stabilization was analyzed for a beam in a plasma-filled waveguide (pgs. 42-43)). Beam trapping calculations usually consider a spectrum of large amplitude waves with one-dimensional wavevector along the beam direction (pgs. 33-34). Nonlinear stabilization mechanisms, such as the parametric modulational instability, have been invoked when the condition for strong turbulence is satisfied (pgs. 34-41). The nonlinear development of parametric instabilities can give rise to Langmuir collapse and soliton and caviton formation (pg. 41). Nonlinear stabilization by weakly turbulent scattering processes is well known (pgs. 41-42).

Since analysis shows that the beam-plasma instability in this experiment is in the strong hydrodynamic regime, the beam can trap rapidly. The growth of beam unstable waves could lead to beam trapping and wave saturation on the time scale of a few linear growth times, which for typical parameters is of the order of a few ns (pgs. 43-44). The beam trapping estimate for the wave energy density indicates a level of unstable waves which is high enough to satisfy the strong turbulent condition for the onset of parametric instabilities (pg. 45). In this experiment, however, electron and ion collisions can be high enough to reduce or even quench the development of these instabilities (pgs 45-48). This means that it is the large amplitude, beam excited modes which take part in the three-wave interaction which produces $2\omega_{pe}$ radiation (pg. 48).

4. The magnitude and scaling of the $2\omega_{pe}$ radiation power is consistent with weak turbulence estimates. Analysis for the parameters of this experiment indicate that the process responsible for the $2\omega_{pe}$ radiation is the three-wave interaction, in which two longitudinal ω_{pe} waves merge into a transverse $2\omega_{pe}$ wave. Kinematics and power estimates are well known for this process within weak turbulence theory (pgs. 53-55). The strongly turbulent state of Langmuir collapse can also lead to $2\omega_{pe}$ radiation. This can occur when the two ω_{pe}

waves in the above three-wave interaction are those which are trapped in cavitons (pg. 56).

The process which produces the $2\omega_{pe}$ radiation in this experiment is the merging of two quasilongitudinal ω_{pe} waves, each excited by one of the beams, into a transverse wave near cutoff with $k_z \sim 0$ (pg. 59). There is no radiation from one beam alone, which argues against a strong turbulence process (pg. 64). Weak turbulence estimates, folding in beam pinching and beam trapping, are remarkably consistent with experiment. Momentum conservation for the three-wave interaction is reflected in the experimental observation of voltage tuning (pg. 59). The scaling of the $2\omega_{pe}$ power with beam current is in reasonable agreement with the observed scalings (pgs. 60-63). The magnitude of the peak power radiated is the same order of magnitude as the experimental value (pg. 61).

3. STANDARD CASE PARAMETERS

To simplify those application sections in which we make numerical estimates and predictions about the mm wave experiment, we chose a "standard" set of parameters. This is a "standard case" of parameters which is representative of the experimental conditions prevailing when data was accumulated for scaling plots. Since many parameters were changed in different runs of the experiment, the parameter space is huge. We can change individual parameters as needed in the application sections.

"STANDARD CASE"

1. Size of waveguide device (refer to Figure 1)

   Length = $L \sim 15$ cm
   Radius = $r_g \sim 1.9$ cm

2. Background neutral gas parameters

   Helium gas
   Pressure = $P \sim 40$ mTorr
   Neutral density = $n_n \sim 1.5 \times 10^{15}$ cm^{-3}

3. Background plasma parameters

   Electron density = $n_e \sim 2.5 \times 10^{12}$ cm^{-3}
   Ion density = $n_i \sim n_e$
   Electron temperature = $T_e \sim 5$ eV
   Ion temperature = $T_i \sim 1/10\ T_e \sim 0.5$ eV
   Plasma frequency = $\omega_{pe} \sim 9 \times 10^{10}$ s^{-1}
   Collisionless skin depth = $\delta_o = c/\omega_{pe} \sim 0.3$ cm
   Electron Debye length = $\lambda_{De} = (T_e/4\pi n_e^2)^{1/2} \sim 10^{-3}$ cm
   Electron thermal speed = $v_{Te} \sim 1.3 \times 10^8$ cm/s
   Electron neutral collision frequency = $\nu_{en} \sim 10^8$ s^{-1}
   Ion neutral collision frequency = $\nu_{in} \sim 10^6$ s^{-1}
   Electron ion collision frequency = $\nu_{ei} \sim 10^7$ s^{-1}

4. Beam parameters

Beam pulse duration = $\tau \sim 20\ \mu s$

Energy of beam one = E_{b1} = energy of beam two = $E_{b2} \sim 30$ keV

Lorentz factor = $\gamma_b \sim 1.06$

Current of beam one = I_{b1} = current of beam two = $I_{b2} \sim 2$ Amp

Ratio of injected beam density to plasma density = $(n_b/n_e) \sim 7 \times 10^{-5}$

Ratio of focused beam density to plasma density = $(\tilde{n}_b/n_e) \sim 6 \times 10^{-4}$

Injected beam cross section = $A_b \sim \pi r_b^2 \sim 7\ cm^2$

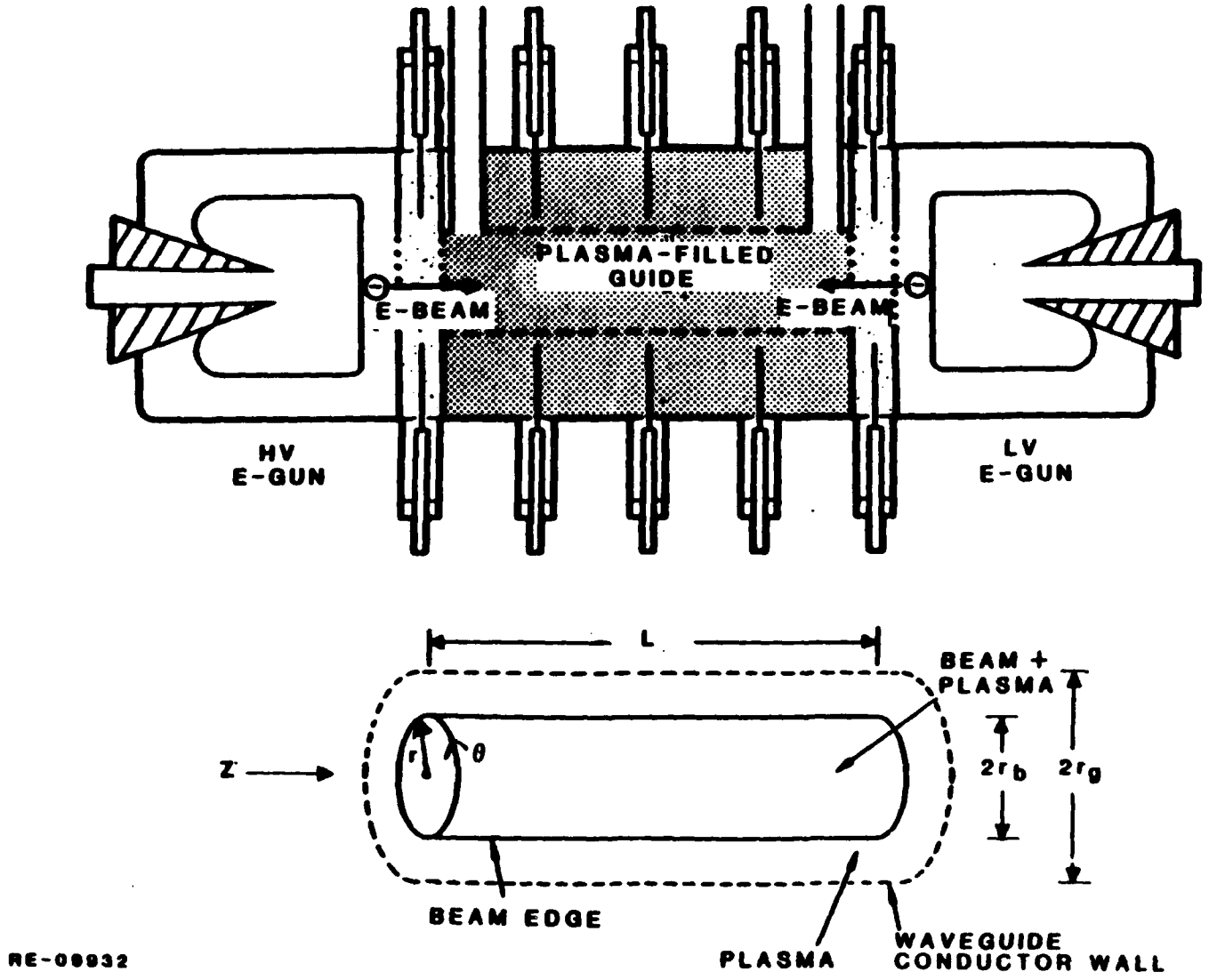

Figure 1. Experimental arrangement and coordinates to be used.

4. SUMMARY AND APPLICATIONS OF LITERATURE

4.1 MAGNETIC SELF FOCUSING

4.1.1 Summary of Literature

4.1.1.1 Bennett Pinch Condition

An electron beam passing through a plasma can magnetically self focus, or pinch, if its current is sufficiently large. The beam tends to spread owing to its perpendicular thermal pressure $n_b T_{b\perp}$, where n_b is the beam density and $T_{b\perp}$ is the perpendicular beam temperature. At the surface of the beam however, the magnetic field B_θ, which is produced by the beam current, generates a magnetic pressure, $B_\theta^2/8\pi$, which tends to constrict the beam. When the magnetic pressure exceeds the thermal pressure, $B_\theta^2/8\pi > n_b T_{b\perp}$, the beam self focuses. (This assumes the plasma has charge neutralized the beam, otherwise the electrostatic forces have to be added to the thermal pressure.) The critical current is given by the Bennett pinch condition, Ref. 1:

$$I_b^2 \geq 3.20 \times 10^{-10}\, n_b A_b T_{b\perp} \qquad (1)$$

where I_b is in amps, n_b in cm^3, $T_{b\perp}$ in eV, and A_b is the cross sectional area of the beam in cm^2. This condition is actually identical to the condition for pinching instabilities in a plasma comprised of two warm counterstreaming electron beams, as discussed in the text by Krall and Trivelpiece, Ref. 2.

Before estimating whether the Bennett pinch condition can be satisfied for a particular beam plasma system, one has to estimate the magnitude of charge and current neutralization of the beam. If the beam charge is not completely neutralized, there is an additional radial electric force in addition to thermal expansion. In addition, the magnitude of beam current neutralization by plasma return currents gives the effective beam current to use in the pinch condition.

4.1.1.2 Charge Neutralization

Charge neutralization occurs on the characteristic time scale $(4\pi\sigma)^{-1}$, where σ is the plasma conductivity. This is the time for plasma charges to

redistribute to nullify the beam E_z field. For a finite length system of length L, in which the beam pulse duration time $\tau >> L/c$, the condition of charge neutrality requires $4\pi\sigma >> (L/a)^2\tau^{-1}$, where a is the beam radius. (See Sudan, Ref. 3.)

4.1.1.3 Current Neutralization

Current neutralization can occur because of Lenz's law. When an electron beam is injected axially into a cylindrical plasma, an induction electric field is generated in the beam head owing to the time rate of change of B_θ as the beam passes a particular position. This induced electric field acts on the plasma electrons to produce a current opposite to the beam current and to reduce B_θ. For a finite length system of length L, in which the pulse duration $\tau >> L/c$, the condition for current neutralization is

$$\tau >> 4\pi\sigma a^2/c^2 \quad , \quad \text{or} \quad \delta_s << a \tag{2}$$

where $\delta_s = (c^2/4\pi\sigma\tau^{-1})^{1/2}$ is the skin depth, Ref. 3. What happens physically is that if the beam radius $a >> \delta_s$, then the beam self field B_θ for $r > a$ is neutralized and E_z vanishes in this region; the electrons outside the radius $r + \delta_s$ are screened from the beam current, which is cancelled by the return current which flows almost entirely within the beam radius. For $a << \delta_s$, this cancellation is only partial because the return current flows both within and outside the beam radius. Other references that discuss plasma return current when a low density relativistic beam is injected into a plasma are Refs. 4-6.

4.1.1.4 Bennett Equilibrium

Macroscopic beam-plasma equilibrium configurations can be investigated starting from the fluid Maxwell equations. Including the effects of finite beam and plasma temperatures, and assuming that (a) the plasma ions form a stationary background, (b) there is no external magnetic field, and (c) beam and plasma centrifugal effects are negligible, these are, Ref. 6:

$$\frac{kT_b}{n_b}\frac{\partial n_b}{\partial r} = -e\left\{E_r - \frac{v_{bz}B_\theta}{c}\right\}$$

$$\frac{kT_e}{n_e}\frac{\partial n_e}{\partial r} = -e\left\{E_r - \frac{v_{ez}B_\theta}{c}\right\} \quad . \tag{3}$$

The Bennett condition follows from this by assuming that $n_e = 0$, $v_{bz}/c = \beta_o$ = constant, and $f_e = n_i/n_b$ = constant; the previous equation then becomes

$$\frac{kT_b}{n_b}\frac{\partial n_b}{\partial r} = \frac{4\pi e^2}{r}(1 - f_e - \beta_o^2)\int_0^r r\,dr\,n_b \quad . \tag{4}$$

When n_b decreases monotonically with radius ($\partial n_b/\partial r \leq 0$), and $\beta_o^2 > 1 - f_e$, then there is an equilibrium configuration in which the outward forces of beam fluid pressure and electrostatic repulsion are balanced by the inward force of magnetic pinching. Then the solution to Eq. (4) is the Bennett profile

$$n_b = n_{bo}\,[1 + (r/a)^2]^{-2} \tag{5}$$

where the Bennett radius is

$$a^2 = \frac{8\lambda_{Db}^2}{\beta_o^2 - (1 - f_e)} \quad , \tag{6}$$

with λ_{Db} the Debye length of the beam electrons. For space charge neutral equilibria,

$$a^2 = \frac{8\lambda_{Db}^2}{\beta_o^2}\left(\frac{T_b}{T_b - T_e}\right) \tag{7}$$

4.1.2 Application to mm Wave Experiment

4.1.2.1 Introduction

The electron beam is focused as it propagates through the waveguide plasma in Schumacher and Santoru's experimental setup. The picture in Figure 2, which is from Ref. 7, shows an example. The beam has converged to an approximate Gaussian profile after passing through the waveguide plasma. The

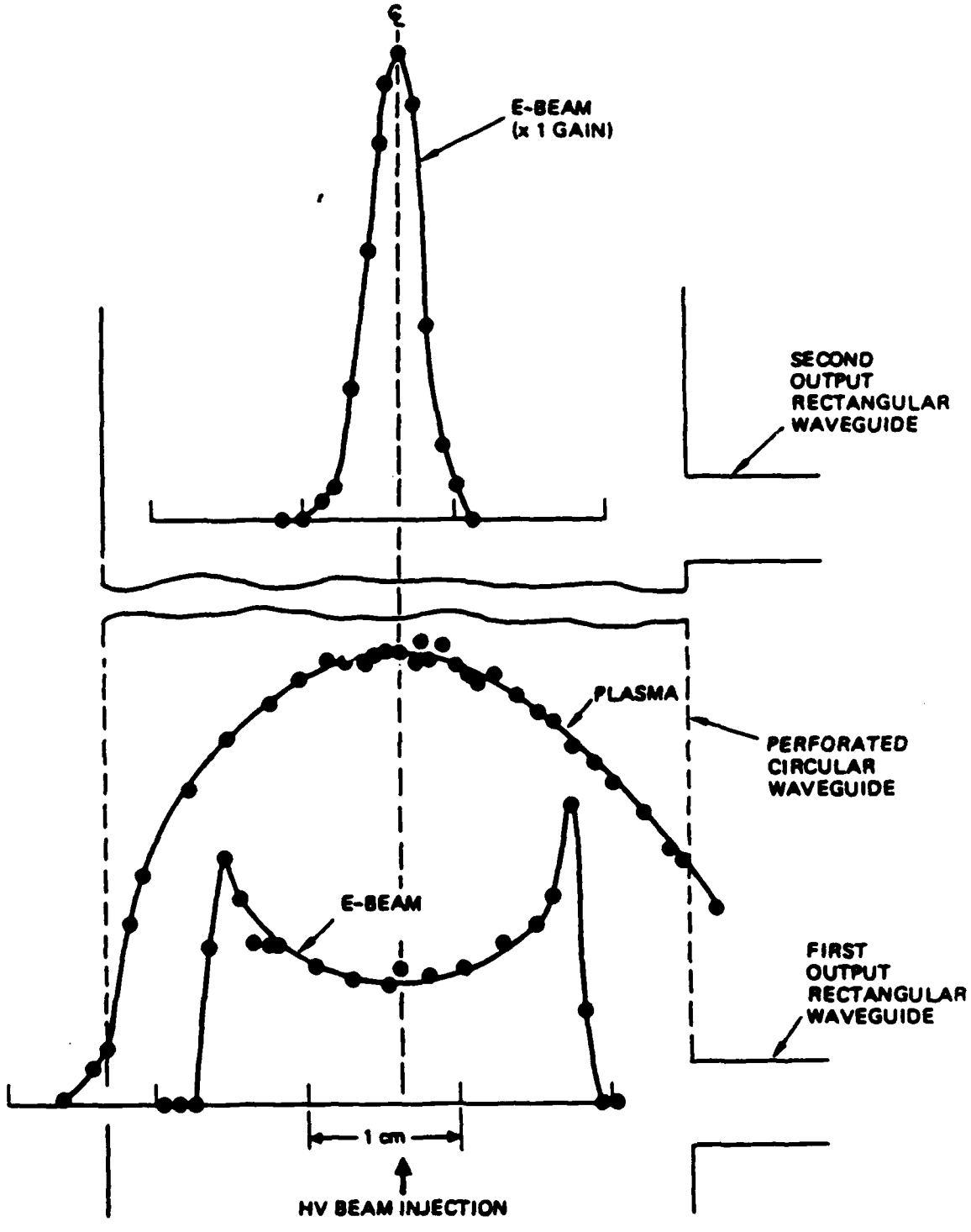

Figure 2. Radial plasma and electron-beam profiles measured across the diameter of the circular waveguide at two axial positions which correspond to the output waveguide locations. (From Ref. 7)

full width at half max decreased from 2.7 to 0.45 cm and the beam current density on axis increased by a factor of ~ 30. We'll investigate whether the beam could magnetically self focus. If this is possible, one could arrange parameters to get optimal focusing. This could lead to (1) stronger beam-plasma instability, because (n_b/n_e) increases, implying a higher energy density of beam unstable plasma waves which could couple to produce a higher power output at $2\omega_{pe}$, and (2) higher emission efficiency at $2\omega_{pe}$, because the efficiency is measured relative to the electron beam energy flux at the input of the guide.

4.1.2.2 Beams are Charge and Current Neutralized

We first estimate the magnitude of charge and/or current neutralization in Schumacher's experiment in order to determine which form of the pinch condition to use and what effective beam current to use. The plasma conductivity will be needed; it can be estimated as

$$\sigma \sim \frac{\omega_{pe}^2}{4\pi \nu_{en}} \tag{8}$$

where ν_{en} is the electron neutral collision frequency, and ω_{pe} is the background plasma density. (The electron neutral collision frequency is larger than the electron ion collision frequency in this experiment, shown later.) The electron neutral collision frequency is

$$\nu_{en} \approx \sigma_{e\text{-}He} n_n v_{Te} \tag{9}$$

where $\sigma_{e\text{-}He}$ is the total elastic cross section of electrons in He, n_n is the density of neutral helium, and v_{Te} is the background electron thermal speed. For $T_e \sim 5$ eV, the cross section is $\sigma_{e\text{-}He} \sim 5 \times 10^{-16}$ cm^2 from the graph in Figure 3, taken from Ref. 8. For the standard case parameters, $\nu_{en} \sim 10^8$ s^{-1}. (For comparison, $\nu_{ei} \sim 3.9 \times 10^{-6}\, n_i \lambda_{ei}/T_e^{3/2} \sim 10^7$ s^{-1} for the standard case.) Thus the conductivity is estimated to be of the order of

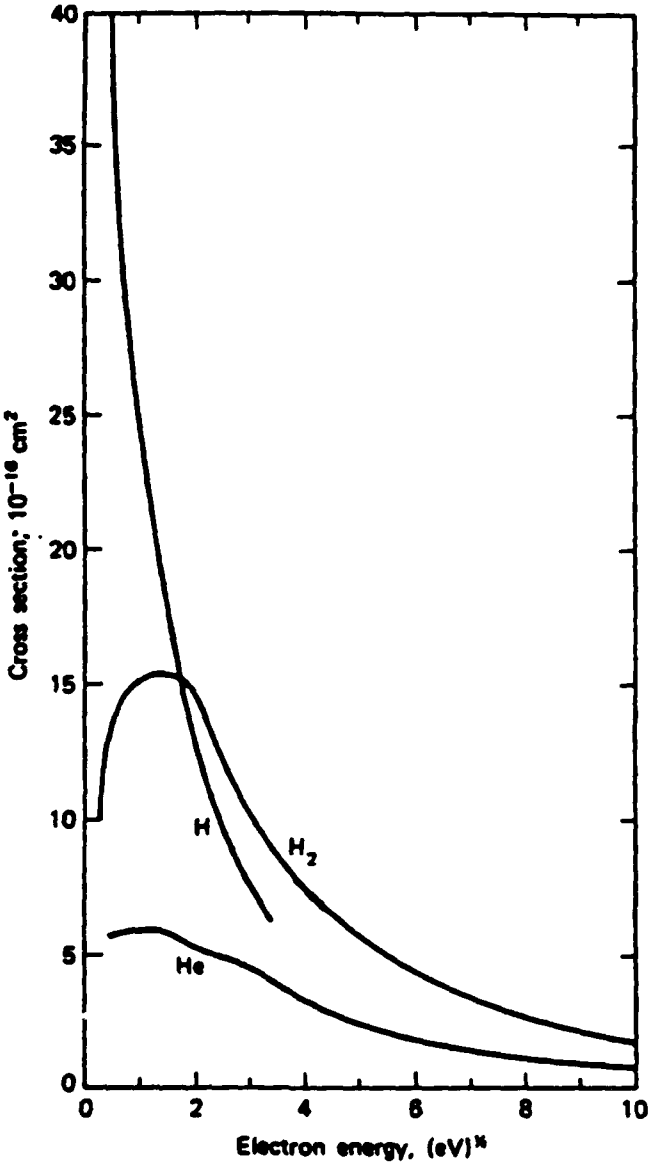

Figure 3. Total elastic collision cross sections of electrons in H, H_2, and He (after Brackmann, Fite, and Neynaber, 1958; and Brode, 1933). (From Ref. 8)

$$\sigma \sim 6.25 \times 10^{12}\ s^{-1} \quad .$$

The charge neutralization condition is $4\pi\sigma >> (L/a)^2\tau^{-1}$. For the standard case, $4\pi\sigma \sim 8 \times 10^{13}\ s^{-1}$, while $(L/a)^2\ \tau^{-1} \sim 3 \times 10^6\ s^{-1}$, so that the condition for charge neutralization is satisfied.

The condition for current neutralization is $\delta_s << a$. Using the standard case parameters, $\delta_s \sim 15$ cm, so that $\delta_s >> a$ and return currents can be neglected.

4.1.2.3 Beam Subject to Bennett Pinch

The condition for the electron beam to pinch and self focus under these conditions can be written from Eq. (1) as

$$\frac{I_b^2}{T_{b\perp}} > 2.26 \times 10^3 \left(\frac{n_b}{n_e}\right)\left(\frac{n_e}{10^{12}}\right)\left(\frac{A_b}{7}\right)$$

with I_b the original beam current. For the parameters in the standard case, the pinch condition would be satisfied as long as

$$\frac{I_b^2}{T_{b\perp}} > 0.4 \quad .$$

For $I_b \sim 2A$ for each beam, the beam could self focus as long as $T_{b\perp} \leq 10$ eV. This is within reason for the experiment. Of course, $T_{b\perp}$ could increase because of collisions, and because of quasilinear stabilization of beam instabilities. The mean free path for these high energy electrons is very long--of the order of 100 cm for electron-neutral collisons when $E_b \sim 30$ keV, so one wouldn't expect much broadening of the transverse temperature distribution due to collisions. Quasilinear stabilization, on the other hand, could lead to broadening of the parallel and perpendicular beam temperatures, as will be discussed in the section on beam stabilization.

4.1.2.4 Bennett Equilibrium

The experimentally measured focused beam profile can be fit with a Bennett profile, Ref. 60. Using the standard case parameters and a measured value of $n_b \sim 3 \times 10^9$ cm^{-3}, this gives a Bennett radius of $a \sim 0.48$ cm for $T_{b\perp} \sim 10$ eV. This is in remarkably good agreement with the Bennett radius value needed for the experimental fit to the Bennett profile. This value of a, moreover, is consistent with the Bennett temperature, that is, that temperature required for pinching to occur.

4.1.2.5 Implications

It appears that the beam self pinches and attains a Bennett equilibrium configuration. The resulting increase of (n_b/n_e) leads to an increased efficiency of $2\omega_{pe}$ radiation, because the radiated power scales as $(n_b/n_e)^p$, where p is some power > 1 which we'll discuss in later sections, while the input power scales as n_b in the unfocused beam.

We note from the pinch condition that, for any temperature, self focusing can be attained by increasing I_b, and thus n_b and/or E_b. If the beam is focused because of the pinch effect, there should be a detectable threshhold. For example, for a beam of low enough current so that $I_b \leq 1$A, we would expect to see no focusing in the standard case because the pinch condition would require the perpendicular beam temperature to be too low, $T_{b\perp} < 2.5$ eV $< T_e$.

4.1.2.6 Work to be Done

Even though it appears that the beam dynamics are fairly well understood in terms of beam pinching and Bennett equilibrium, there are topics which need further investigation. These include (a) analysis of loss mechanisms which prevent $T_{b\perp}$ from increasing above the Bennett temperature, (b) effects of beam-beam coupling on beam dynamics, (c) evaluation of parameter regimes in which return currents, and their effects on beam pinching, need to be considered, (d) effects of vertical magnetic fields on beam pinching, and (e) optimization of beam focusing with respect to the strength of the beam-plasma instability and the three-wave interaction power output.

4.2 BEAM-PLASMA AND TWO-STREAM INSTABILITIES

4.2.1 Summary of Literature

4.2.1.1 Introduction

There have been a multitude of papers on beam-plasma and two-stream instabilities. We take beam-plasma to refer to the interaction of a low density, $(n_b/n_e) << 1$, beam with a background plasma, while two-stream will refer to counterstreaming plasmas with near equal densities. The papers relevant to Schumacher and Santoru's experiment comprise a small subset. These include papers on beam-plasma instabilities in a plasma in a waveguide, which take into account the finite radial, and rarely, the finite axial extent of the system, as well as a few papers concerned with the instability of a system of two counterstreaming electron beams in a background plasma. Several of the papers we describe below overlap the various subsections.

4.2.1.2 Beam-Plasma Instabilities in a Plasma-Filled Waveguide

First we discuss some results on beam-plasma instabilities in a plasma-filled waveguide, with and without an axial magnetic field.

a. Beam Radius = Guide Radius: Axisymmetric Modes

References 9-11 are referred to as Aronov (a)-(c). Aronov (a) analyzes beam-plasma instabilities arising when a relativistic low density beam is injected into a plasma-filled waveguide, as well as beam relaxation by quasilinear processes, and electromagnetic radiation produced by the beam-plasma instability. Longitudinal waves are not eigenmodes of this beam-plasma system: the beam excites arbitrary non-electrostatic modes. The unstable waves have a small electromagnetic component which produces a finite Poynting flux, and thus electromagnetic radiation. The model system in (a) is a uniform plasma-filled cylindrical waveguide with a low density electron beam of radius equal to the guide radius. All components are cold, and the beam can be relativistic. In this finite radial system the dispersion equation describes an electromagnetic field with nonvanishing components E_r, E_z and B_θ, with

$$E_z = \sum_n E_{zn}(r)\, e^{-i\omega t + ik_z z} = \sum_n E_{zn} J_o\left(\frac{\mu_n r}{r_g}\right) e^{-i\omega t + ik_z z} \qquad (10)$$

where r_g is the guide radius, and $E_r(r)$ and $B_\theta(r)$ are related to $E_z(r)$. There are two types of unstable solutions. One is the analog of the Cerenkov type instability in an infinite plasma, which occurs as a result of a resonant interaction between an electron beam mode and a waveguide mode, in which the condition $\omega = \underset{\sim}{k} \cdot \underset{\sim}{v}_b$ is satisfied. This results in the excitation of a quasi-longitudinal wave with a spectrum

$$\omega_n = k_z v_b + i\delta_n = \omega_{pe} + i\delta_n$$

$$\delta_n = \left(\frac{\sqrt{3} - i}{2}\right) \omega_{pe} \left(\frac{n_b}{2\gamma_b n_e} \frac{\mu_n^2 + k_z^2 r_g^2 \gamma_b^{-2}}{\mu_n^2 + k_z^2 r_g^2}\right)^{1/3} \qquad (11)$$

where μ_n/r_g is essentially the radial wavenumber $k_{\perp n}$, with the azimuthal wavenumber being zero because the mode is described by the axisymmetric J_o, and k_z is the axial, or longitudinal wavenumber, r_g is the waveguide radius (and thus the beam radius), γ_b is the Lorentz factor for the beam, $\gamma_b = [1 - (v_b^2/c^2)^{-1/2}]$. For $\gamma_b = 1$, there is no dependence of the growth rate on the radial wavenumber, but for $\gamma_b >> 1$, the growth rate maximizes for short radial wavelengths, $k_\perp^2 >> k_z^2$. The radial wavenumber is discrete, and there is a minimum $k_\perp \approx 2.4/r_g$. The unstable wave is essentially electrostatic, with $E_{rn} \approx (k_{\perp n}/k_z)E_{zn}$, with a small departure from electrostatic behavior due to the finite magnetic field of the wave

$$B_{\theta n} \approx \frac{\delta_n}{\omega_{pe}} \left(\frac{v_b}{c}\right) E_{rn} \quad . \qquad (12)$$

The other unstable solution corresponds to a wave propagating at nearly right angles to the beam directed velocity, i.e., in the limit $k_z \to 0$ or $|\omega| >> k_z v_b$, where v_b is the beam directed speed. This is an aperiodic, Weibel type instability, with growth

$$\omega \approx \frac{iv_b}{c}\frac{\omega_{pe}}{\sqrt{\gamma_b}}\left(\frac{n_b}{n_e}\ \frac{c^2\mu_n^2}{c^2\mu_n^2 + r_g^2\omega_{pe}^2}\right)^{1/2} \quad . \tag{13}$$

This instability is similar to the hydrodynamic sausage instability and corresponds to the constriction of the plasma into individual filaments.

Aronov (b) generalizes the results of (a) to the case of a magnetoactive plasma in a waveguide. Aronov (c) investigates the conditions under which an electron beam injected into a waveguide excites only a single mode with a narrow linewidth. In the process they review work on the interaction of relativistic electron beams with plasmas, including the effect of finite radial dimensions. Both unstable volume and surface waves are considered. (This was done to investigate the possibility of using beam plasma systems to produce high power generators and amplifiers of electromagnetic radiation, using the fact that the beam excited waves are inherently electromagnetic.) Recent refinements on beam-plasma instability in waveguides have included the effects of an external magnetic field and finite beam temperature. See Refs. 12-17.

b. Beam Radius = Guide Radius: Non-Axisymmetric Modes

We review aspects of Tajima's paper, Ref. 17, which are relevant to Schumacher and Santoru's experiment. The stability of a relativistic electron beam-plasma system in finite (cylindrical) geometry is investigated. The analysis is based on collisionless fluid theory. By employing the full set of Maxwell's equations, both finiteness and relativistic effects are included. One of the cases analyzed is the bounded beam-plasma system with no external magnetic field, and with both beam and plasma radius equal to the waveguide radius (conductor surface). The result generalizes Aronov's results to non-axisymmetric modes, that is, finite m in a representation of the electromagnetic field component as

$$E_{zmn}(r) = E_{zn}(r)\ J_m\left(\frac{\mu_{mn} r}{r_g}\right) \quad . \tag{14}$$

(Compare with Eq. 10.) For a nonrelativistic beam, the results for both the Cerenkov type beam-plasma instability and the filamentary, or Weibel

instability, are similar in form to Aronov's results, and indeed, to the infinite plasma result. There is not a significant stabilizing effect by the finiteness of the system. The modes are merely quantized in the radial direction: that is, $k_{\perp mn} = (\mu_{mn}/r_g)$ has to satisfy $J_m(\mu_{mn} r_g) = 0$.

c. Beam Radius << Guide Radius: Axisymmetric Modes

Another relevant case in Tajima's paper is a thin beam in a bounded plasma, in which the beam radius is much smaller than the plasma radius. For the Cerenkov beam-plasma instability, the modes with higher azimuthal mode number m in this case can be neglected; the plasma eigenmodes with higher m cannot couple with the beam at the center of the plasma, where the plasma eigenmode amplitude vanishes for $m \geq 1$, that is, for $E_z(r = 0) = 0$ for $m \geq 1$. (This effect has been observed experimentally for a weak nonrelativistic beam in Ref. 18.) The strength of this instability decreases with increasing axial magnetic field and decreasing plasma radius. In addition, the strength of the instability is characterized by the integrated beam density over the entire plasma cross section, instead of by the local plasma density. (That is, what enters in the dispersion relation is not the local density of the beam, but the integrated beam density over an entire cross section of the plasma with the 0th order Bessel function as a weighting factor.) This would imply that a pinched beam would not have a much stronger interaction than an unpinched beam. Tajima also discusses the surface filamentary instability for a thin hollow beam, finding strong dependence of the growth rate on the azimuthal mode number, with strength determined again by the integrated total current.

d. Arbitrary Beam Radius: General Modes

A recent analysis of beam-plasma instabilities in a bounded plasma was published by Michael E. Jones in Ref. 19. The paper reports on a linear eigenfunction analysis of the beam-plasma instability for an annular beam interacting with a plasma which fills a coax line. The geometrical configuration is shown in Figure 4. The dispersion matrix, however, contains various limits including the cylindrical waveguide (no center conductor, $r_c \to 0$), a solid beam ($r_i \to 0$), both thin ($r_e << r_d$) and fat beams ($r_e = r_d$), and the infinite plasma case ($r_d \to \infty$). The beam and plasma are modelled by relativistic cold fluids, including collisions, and the dispersion relation is

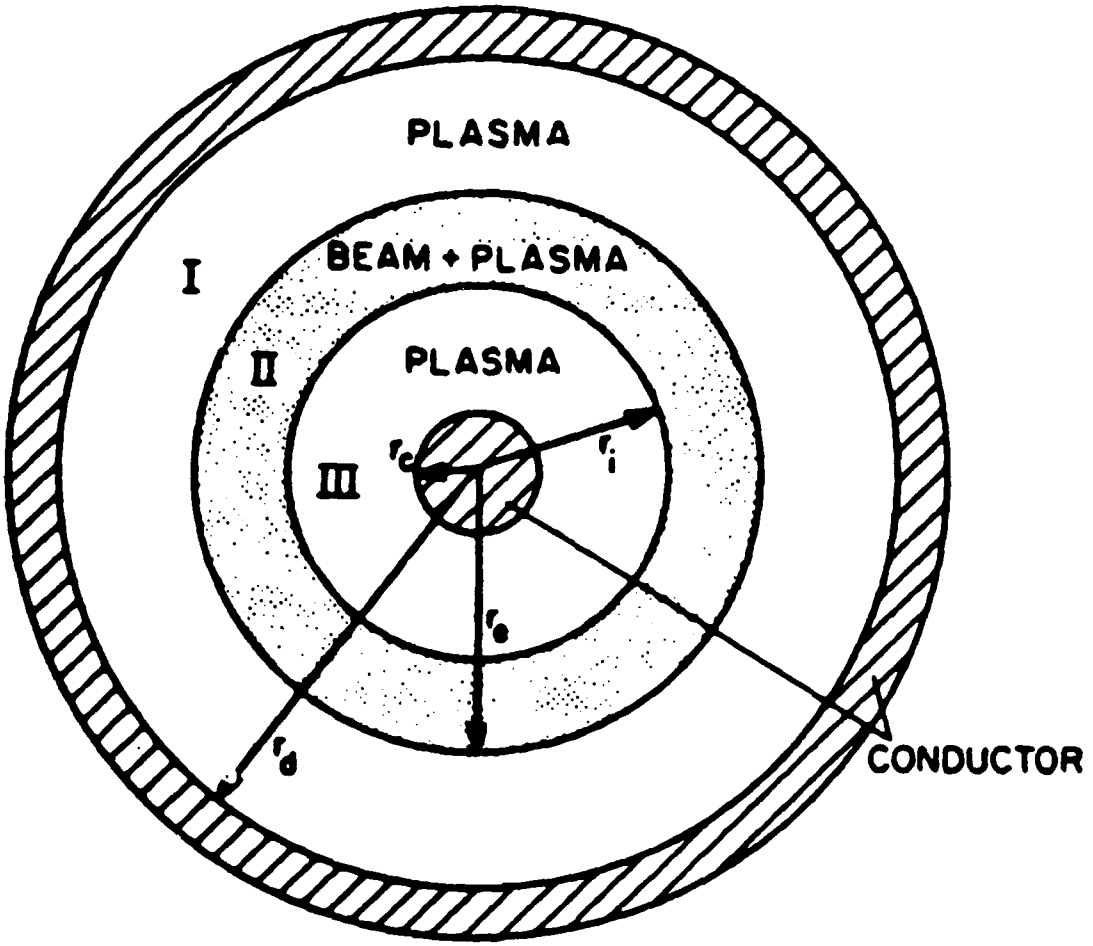

Figure 4. Most general geometrical configuration considered in the analysis. (From Ref. 19)

three-dimensional and electromagnetic. The radial eigenfunction structure is discussed and numerical examples are given for a particular parameter regime corresponding to a very dense plasma (10^{17}-10^{20} cm^{-3}), in which the radial size of the coax plasma is of the order of 35 collisionless skin depths δ_0 ($\delta_0 = c/\omega_{pe}$), the thickness of the annular beam is 15 δ_0, and $(n_b/n_e) \sim 10^{-3}$, with $\gamma_b \sim 7$.

These are the general trends which emerge from this analysis in Ref. 19 and which give some insight into the behavior of beam-plasma instabilities in a bounded plasma. For the case of a solid beam filling the waveguide or drift tube (no center conductor) the TE and TM modes decouple, with the unstable modes being the TM modes. The dispersion relation reduces to the one given by Tajima in Ref. 17. In this case, when the uniform beam and plasma have the same radial profile and are in contact with conductors, the only effect of finite radial dimensions is to quantize the perpendicular wave vectors. However, when the profiles are different, and the beam is thinner, this quantization is complicated by other effects. For example, for non-axisymmetric modes ($m \neq 0$) the TM and TE waves are coupled (although the coupling is weak for small (n_b/n_e)). Also, surface like waves appear whose eigenfunctions are largest at the beam edges. Unstable waves are evanescent outside the beam radius, so that the quantization of the perpendicular wavevector is determined by the beam thickness.

Numerical results for a typical spectrum for the unstable modes of the general geometry system, shown in Figure 5, are qualitatively the same as would be obtained for the infinite homogeneous system. The growth rate maximizes at $k_z v_b \sim \omega_{pe}$, which corresponds to the Cerenkov instability, which is nearly electrostatic. The part of the spectrum at $k_z = 0$, referred to as the electromagnetic Weibel, or filamentary, instability, is associated with an increase in the magnetic components of the eigenfunctions. The eigenfunctions corresponding to the peak growth rate in Figure 5 are shown in Figure 6 [$r_m = (r_e + r_i)/2$ and $m = 10$]. Figure 7 shows the dependence of the growth rate on k_r or $k_\perp$ for $m = 0$. The modes of the finite system can be correlated with the modes of the homogeneous system with a suitable quantization of the perpendicular wave vector. In addition, if the conductors are more than a couple of collisionless skin depths distant from the beam, the modes are virtually unaffected by their presence. But when the conductors are closer,

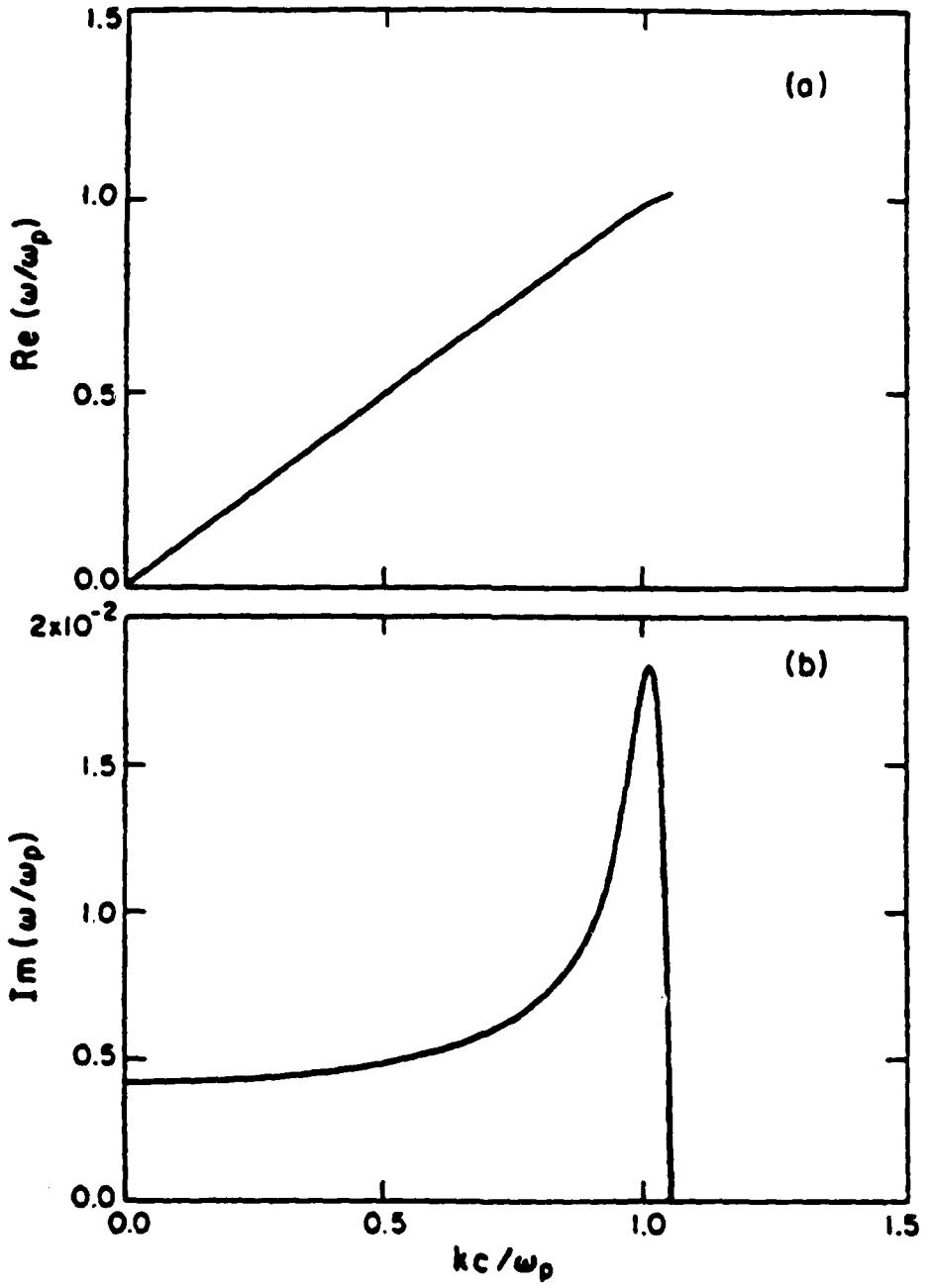

Figure 5. Spectrum for the first unstable bulk mode. (From Ref. 19)

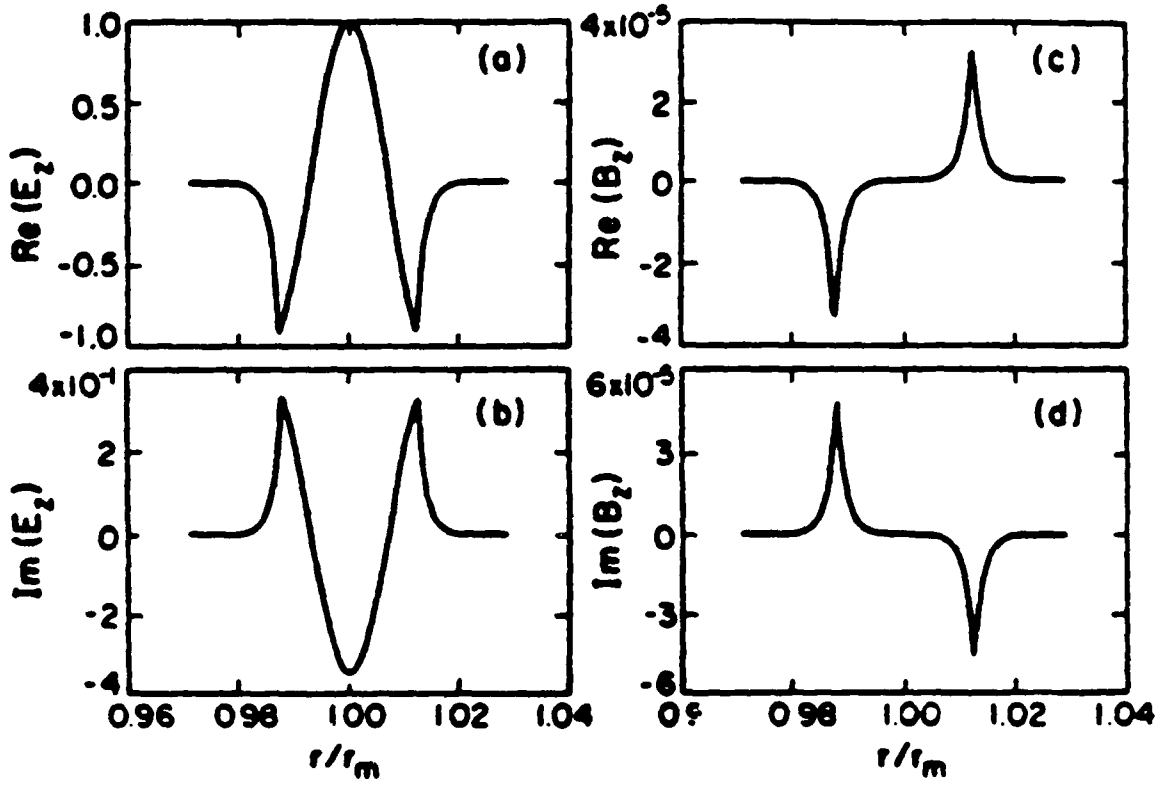

Figure 6. Eigenfunctions for the first bulk mode at peak growth rate. (From Ref. 19)

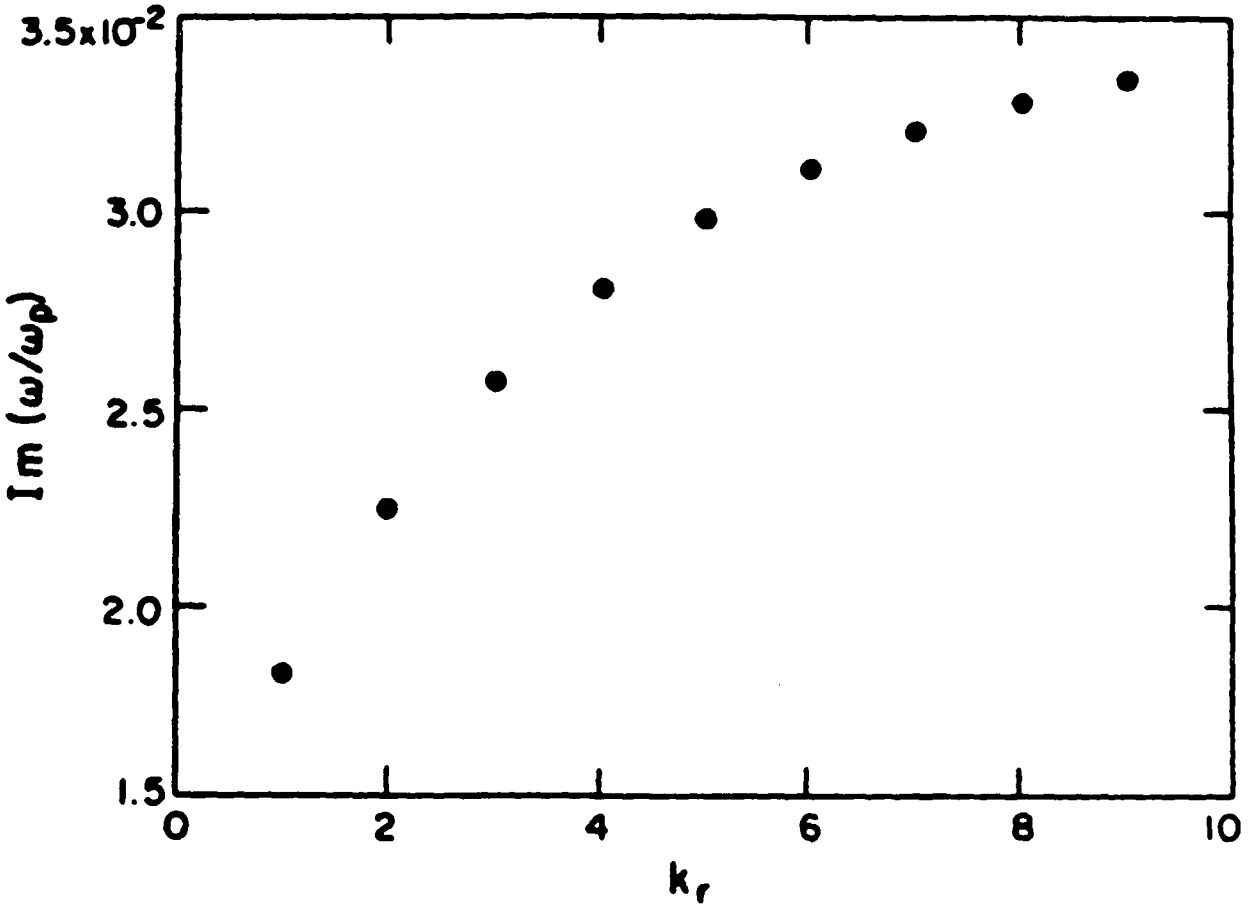

Figure 7. Growth rate scaling as a function of the number of radial oscillations. (From Ref. 19)

the electric field of the eigenfunctions has to go to zero more rapidly outside the beam and the growth rate is reduced.

Jones also presents several particle-in-cell (PIC) simulations in order to test the validity of the eigenfunction analysis. This is because there is some question about how smooth the radial profiles can be before the continuous spectrum alone determines the response of the system, and eigenfunctions don't exist (Ref. 20). It was shown in Ref. 21 that radial eigenfunctions do exist in the system that Jones studied provided that the beam profile is not too smooth. The PIC simulations indicate that while the eigenfunctions probably do not describe the entire response of the system, many of the features of the analysis were oberved in the simulations. The quantitative agreement between simulation and linear theory was estimated to be about 50% for the growth rate, which Jones considers adequate considering the effect of numerical collisions.

e. Convective Instability

All the papers referred to above assume that k is real and that ω is imaginary, that is, that the instability is absolute. In an infinite plasma, of course, the beam-plasma instability can have both temporal and spatial growth. For a cold beam, under the conditions $(T_b/E_b)^{1/2} \ll (n_b/2n_e)^{1/3} \ll 1$, the temporal growth is given by $\delta \sim \sqrt{3/2}\,(n_b/2n_e)^{1/3}\omega_{pe}$; while for a cold beam, under the conditions $(T_b/E_b)^{1/2} \ll (n_b/6n_e)^{1/3}(E_b/T_e)^{1/3} \ll 1$, the spatial growth is given by $k_I \sim \sqrt{3/2}\,(n_b/6n_e)^{1/3}(E_b/T_e)^{1/3}(\omega_{pe}/v_b)$, Ref. 22. When the plasma and beam are both stone cold, i.e., zero temperature, the instability is absolute, Refs. 23-24.

A review by Bers (Ref. 24) covers topics in the space-time evolution of plasma instabilities. In one section, he discusses the question of convective versus absolute instability for the electrostatic instability in a 1-D model of counterstreaming beams propagating through a plasma. We summarize this here. The unperturbed particle distribution functions have Lorentzian shapes:

$$f_e(v) = (\alpha_e/\pi^2)\,\frac{n_e}{(v^2 + \alpha_e^2)^2}$$

$$f_b(v) = \frac{(\alpha_b/\pi^2)n_b}{(|v - v_b|^2 + \alpha_b^2)^2} + \frac{(\alpha_b/\pi^2)n_b}{(|v + v_b|^2 + \alpha_b^2)^2} \quad . \qquad (15)$$

The plasma particles have density n_e, with α_e a measure of their velocity spread. The two beams each have density n_b and velocity spread α_b around v_b, the drift velocity. For electrostatic waves with k along v_b, the linearized Vlasov-Poisson equations lead to the following two dispersion relations:

$$D_{\pm}(k,\omega) = 1 - \frac{\omega_{pe}^2}{(\omega \pm ik\alpha_e)^2} - \omega_b^2 \left[\frac{1}{(\omega - kv_b \pm ik\alpha_b)^2} + \frac{1}{(\omega + kv_b \pm ik\alpha_b)^2} \right] \tag{16}$$

Here $D_+(k,\omega)$, $D_-(k,\omega)$, are valid for $\mathrm{Im}(\omega/k) > 0$, $\mathrm{Im}(\omega/k) < 0$, respectively. This dispersion relation applies to two counterstreaming electron beams propagating through a background unbounded plasma. The main results of a numerical stability analysis of this dispersion relation follows, Refs. 25 and 26. When $\alpha_e = \alpha_b = 0$ (cold plasma and cold beams), there are two possible absolute instabilities: one at $\omega = \omega_{pe}$, and one at $\omega = i\omega_b[(1/4) - (\omega_{pe}/\omega_b)^2]^{1/2}$, which is unstable only if $(\omega_p/\omega_b) < 1/2$. For $(\omega_p/\omega_b) > 1/2$, the solution is dominated by the instability at $\omega = \omega_{pe}$ (the beam-plasma instability), while for $(\omega_p/\omega_b) < 0.2$ it is dominated by the other instability (the two-stream instability; for $\omega_{pe} = 0$, one has the case of two counterstreaming beams). For $0.2 < (\omega_p/\omega_b) < 1/2$ the two instabilities interact. It appears that this would not be important for Schumacher and Santoru's experiment, because $(n_b/n_e) \ll 1$. Finite velocity spreads, $\alpha_e \neq 0$ and $\alpha_b \neq 0$, have different effects on these two types of instabilities. For $\omega_{pe} = 0$, i.e., counterstreaming beams, increasing α_b reduces the two-stream growth rate, until this absolute instability vanishes at $\alpha_b = v_b$; at instability threshhold (i.e., $\alpha_b \leq v_b$) the instability is absolute. For $(\omega_p/\omega_b) < 1/2$, increasing α_b rapidly reduces the growth of the two-stream, but to a much lesser extent, the beam-plasma growth rate. Increasing α_e has the opposite effect in this regime; it can even increase the growth of the two-stream. For $(\omega_{pe}/\omega_b) > 1/2$, increasing α_b reduces the growth of the beam-plasma instability but it remains absolute; finite α_e, on the other hand, makes the instability convective. This latter regime may be the relevant one for the mm wave experiment.

Reference 27 investigates counterstreaming instabilities arising in three component electron plasmas both analytically and numerically. This is a general non-symmetric case in which two beams of unequal density and unequal drift velocity counterstream through a background plasma. The analysis is for an infinite homogeneous plasma, and only longitudinal modes are considered. The parameter region investigated corresponds to $(n_p/n_b) < 1$. The spectrum of the two-stream instability, which occurs in the symmetric counterstreaming beam case without background plasma, can be transformed into wave spectrum having a complex structure; the instability changes from absolute to mixed convective and absolute.

4.2.2 Application to mm Wave Experiment

4.2.2.1 Introduction

We apply quantitatively some of the results discussed in the summary above to Schumacher and Santoru's experiment. Section (e) in the summary above discusses the nature of the instabilities arising in a system of two counterstreaming beams in a plasma. For $(n_b/n_e) << 1$, the solution is dominated by the instability at ω_{pe}, that is, the Cerenkov beam-plasma instability of each beam. (There may be coupling in the small k_z limit, $k_z \to 0$, which affects the Weibel, or filamentation instability, but this has a lower growth rate.) In the following, we'll concentrate on the beam-plasma instability.

4.2.2.2 Beam in Plasma-Filled Waveguide: Beam Radius = Guide Radius

Equation (11) gives the growth rate for the Cerenkov beam-plasma instability under the conditions assumed in Aronov (a), Ref. 9. The growth rate increases slightly with $k_\perp$ because of the presence of the γ_b factor in the growth rate. There is a minimum $k_\perp$ which is $k_\perp = 2.4/r_g$, where r_g is the waveguide radius. For the standard case, $k_\perp \sim 1.26\ cm^{-1}$. The axial wavenumber k_z is given by $k_z = \omega_{pe}/v_b \sim 9\ cm^{-1}$. For the standard case, the growth rate is of the order of $\delta \sim 0.07\ \omega_{pe} \sim 6 \times 10^9\ s^{-1}$ for the lowest order axisymmetric mode, with growth increasing only very slightly as the number of nodes in the radial eigenfunction increases. There is plenty of time for an instability to

develop, since a growth period is of the order of 0.2 ns in this example, and the beam is on for ~ 20 μs. This unstable mode is quasilongitudinal, and essentially electrostatic, with $E_r \sim (k_\perp/k_z)E_z$, so that for this lowest order mode $E_r \sim 0.14\ E_z$, and the electric field of the mode is predominantly in the axial direction. The small departure from electrostatic behavior is due to the magnetic field of the wave; in this case, $B_\theta \sim 0.02\ E_r$.

The Weibel, or filamentary instability, in the limit $k_z \to 0$, has a growth rate which increases as $k_\perp$ becomes much larger than the inverse collisionless skin depth. The collisionless skin depth for the standard case is $\delta_0 \sim 0.3$ cm, while for the lowest order axisymmetric mode, $k_\perp \sim 1.26\ cm^{-1}$ so that the growth rate is not a maximum for this mode. In fact, the growth of the aperiodic instability would maximize for $\mu > 8$, that is, for axisymmetric modes whose radial eigenfunctions have more than 3 nodes. The ratio of the maximum growth rate of the filamentary to the Cerenkov instability is of the order of 0.1 for the standard case.

4.2.2.3 Thin Beam: Axisymmetric Modes

When the beam is very thin, and concentric with the guide, the modes that are excited should be axisymmetric TM_{0np} modes. This is because the waveguide modes for $m \geq 1$ have $E_z(r=0) = 0$, and therefore can't couple with the beam. The stabilizing effect of the wall can be estimated by comparing the magnitude of the collisionless skin depth in the plasma to the distance of the beam edge from the wall. For the standard case, $\delta_0 \sim 0.3$ cm. If the beam focuses to an effective radius of 0.5 cm in the interaction region say, then the distance between beam edge and waveguide wall is 5 - 6 collisionless skin depths, so that one would not expect strong stabilizing influences from the wall. Note, however, that as the plasma density decreases, the collisionless skin depth increases as $n_e^{-1/2}$, and the stabilizing effect of the wall conductor might be felt. If the background plasma density were $2 \times 10^{11}\ cm^{-3}$, the beam edge would be ~ $1\delta_0$ from the guide wall, whose stabilizing effect could lower the growth rates. It appears then, that a highly focused, thin beam can be strongly unstable in even a low density plasma, while a weakly focused, fat beam needs a higher density background plasma to provide more shielding between it and the stabilizing conducting wall of the guide.

4.2.2.4 Thermal Effects on Beam-Plasma Instability: Limits on $k_\perp$

Beam temperature effects cut off these beam plasma instabilities when the longitudinal and/or transverse spread of the electron velocities in the beam are large enough so that

$$|\delta|^2 < k_z^2 (\Delta v_{b\parallel})^2 \quad , \quad k_\perp^2 (\Delta v_{b\perp})^2 \quad ,$$

where $(\Delta v_{b\parallel})^2 = T_{b\parallel}/m_e\gamma_b^6$ and $v_{b\perp}^2 = T_{b\perp}/m_e\gamma_b^2$ are the longitudinal and transverse beam electron speeds, and $T_{b\parallel}$ and $T_{b\perp}$ are the longitudinal and transverse beam temperatures. The condition $\delta < k_z(\Delta v_{b\parallel})$ could be satisfied if $(\delta/\omega_{pe}) < (T_{b\parallel}/E_b)^{1/2}$, which could put an upper bound on $T_{b\parallel}$. Since $(\delta/\omega_{pe}) \sim 0.07$ for the standard case, this implies that $T_{b\parallel} \lesssim 150$ eV in order for the Cerenkov instability to go.

The condition $\delta < k_\perp v_{b\perp}$ puts a limit on the magnitude of either $k_\perp$ for fixed $T_{b\perp}$, or $T_{b\perp}$ for fixed $k_\perp$. For example, for fixed $k_\perp \sim 2.4/r_g \sim 1.26$ cm^{-1}, this implies that $T_{b\perp}$ has to be < 2 keV for the standard case. On the other hand, if $T_{b\perp} \sim 10$ eV, then all $k_\perp < 30$ cm^{-1} can be unstable. Since $k_\perp = \mu/r_g$, this implies that a large number of modes can be unstable for realistic setups. In general, then, it appears that the unstable spectrum in $k_\perp$ is quite broad, decreasing in width as the beam thickness decreases. The k_z spectrum, on the other hand, is quite narrow, of the order of $\Delta k_z \sim (n_b/n_e)^{1/3} k_{zo}$ in the linear regime: for the standard case, this width is of the order of $0.08\ k_{zo}$.

4.2.2.5 Quantization of k_z

We make a point about the quantization of k_z in Schumacher's experiment. Because the endplates of the drift tube are actually constructed of the same material as the cylindrical walls (porous conductors so that electrons can get in but waves can't get out), the setup is more like a cavity resonator. As such, k_z, which can take arbitrary values for a waveguide, has to take discrete values in order to satisfy the boundary conditions on the

electromagnetic fields at the walls $z = 0$ and $z = L$. This implies $k_z L = p\pi$, where p is an integer. Fields inside such a cavity are set up in such a way as to allow integral half cycles of variation in the axial direction owing to the boundary conditions. A good discussion of the solutions of the wave equations, boundary conditions, and mode solutions for various cavity resonators is given in Ref. 28. Now even though k_z is quantized, the spacing between the allowed values are small enough so that the Cerenkov resonant condition could be satisfied; that is, $\pi/L < (n_b/n_e)^{1/3} k_z$, the latter being the width of the spectrum in k_z at maximum growth. For example, $\pi/L \sim 0.2$ cm^{-1} for the standard case, while $(n_b/n_e)^{1/3} k_z \sim 0.7$ cm^{-1}, so that the Cerenkov condition can be satisfied. We note that there may be no resonant Cerenkov instability if the plasma density is too low or if the beam energy is too high. This could be realized for example, if n_e were $\sim 2 \times 10^{11}$ cm^{-3}, and E_b were ~ 90 keV; then $\Delta k_z \sim 0.1$ cm^{-1}, and $\pi/L > \Delta k_z$. One would expect lower growth at these parameters than in the infinite plasma case, but it's hard to see how to verify this expectation experimentally in the mm wave experiment.

4.2.2.6 Work to be Done

We think that the direction for immediate theoretical work is to include a counterstreaming beam into Michael Jones's (or possibly Toshi Tajima's) analysis and grind out results for parameter regimes appropriate for Schumacher's experiment. The eigenfunction analyses appear to agree with particle-in-cell simulations to within a factor of ~ 2 for the growth rates (M. E. Jones, Ref. 19). In addition, Jones has shown that discrete eigenfunctions and spectra do exist provided that the beam and plasma profiles are not too smooth. In Schumacher and Santoru's experiment, it appears that the plasma profile is fairly flat radially, as shown in Figure 8, and can be taken essentially uniform: the beam profile is quite peaked centrally at least at the opposite end of the waveguide to injection, and may possibly be approximated as a uniform step. If continuous spectra were dominating the plasma response, one would expect to see the ramifications of this in the $2\omega_{pe}$ radiation in the mm wave experiment; that is, one would expect to see a broad spectrum of radiation, and this does not appear to be the case. Furthermore,

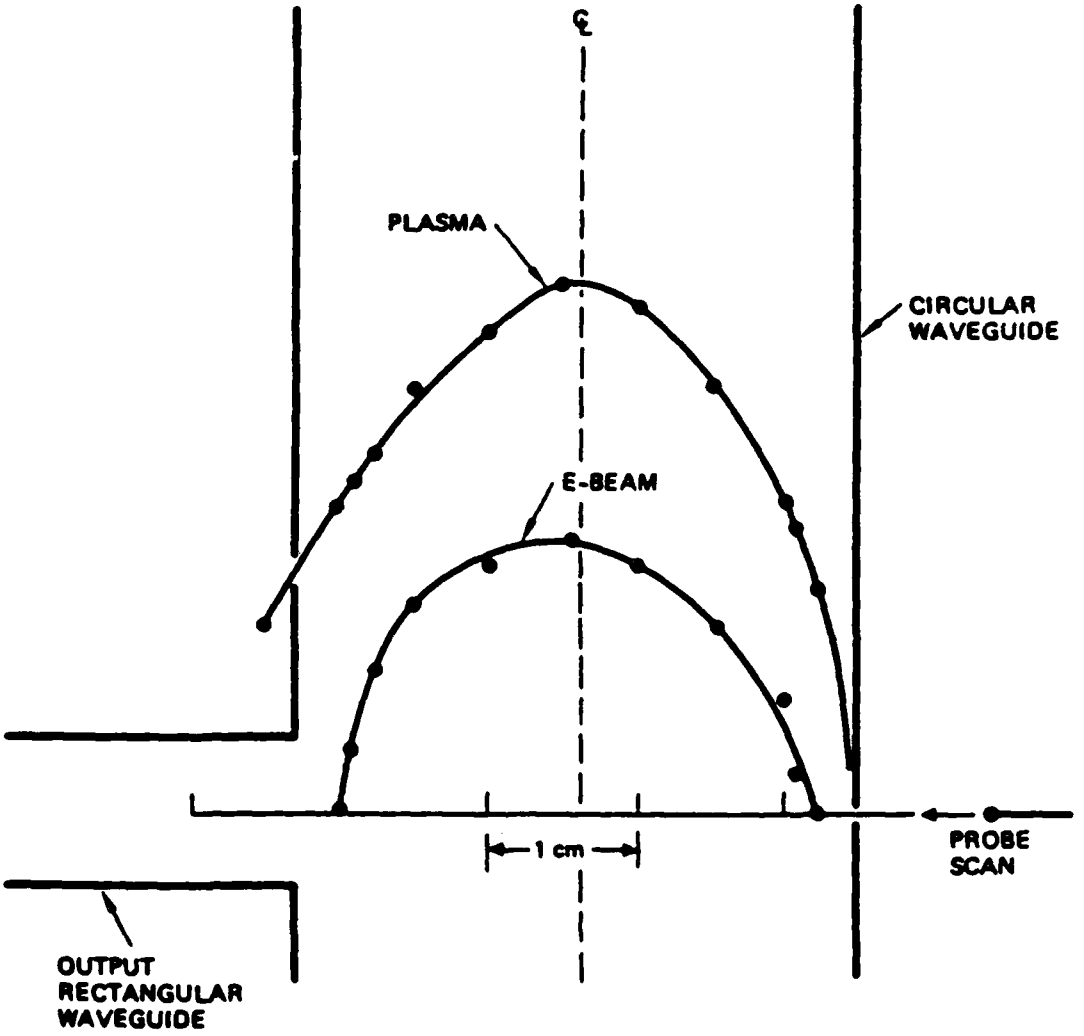

Figure 8. Electron-beam and plasma profiles measured across the diameter of the waveguide in the output-coupling section. (From Ref. 7)

it would appear to be cleaner and faster to apply available eigenfunction analysis literature to the problem, and to then include other effects if the computed growth rates lead to gross inconsistencies in comparing theory with experiment.

We think that the results of an eigenfunction analysis, neglecting temperature effects, might lead to the following results in general. Since $(n_b/n_e) << 1$, the beam-plasma Cerenkov instability will dominate for finite k_z, with a growth rate symmetric in k_z, that is, the same for both the forward and the backward propagating unstable waves (assuming equal energy and density beams). The growth rate for each beam would be given by Jones's one beam result, Ref. 19, in the appropriate beam-plasma geometrical configuration, with the replacement of k_z with quantized k_z, because the drift tube in the mm wave experiment is actually a cavity. We need to work out the growth rates for the parameter regimes of interest for the mm wave experiment. We should investigate both bulk and surface modes. An additional geometrical complication would be the case in which the beams are both off center, as in the experiments with a vertical magnetic field, Ref. 60.

Couplings might occur between beam instabilities in the small limit, $k_z \to 0$, for the filamentary instability, and we will have to work this out. Because of finite temperature, we will need to investigate the convective nature of the instability as well. This could possibly be done within this analysis by keeping ω real and solving for complex k. We haven't determined at this point whether the instabilities in Schumacher's experiment are absolute or convective in nature, or both, but we make a point here. In Schumacher and Santoru's experiment, there are boundary conditions that have to be satisfied by the electromagnetic fields, because of the finite radial and also the finite axial dimensions of the drift tube. This would imply that both $k_\perp$ and k_z would have to be real in order to satisfy these conditions.

4.3 BEAM STABILIZATION

4.3.1 Summary of Literature

4.3.1.1 Introduction

Beam stabilization in a bounded plasma has been treated very little in the literature. Much theoretical work has been done, however, for the beam in an infinite homogeneous plasma. The main relevant mechanisms include beam trapping, nonlinear stabilization in either the strongly turbulent or weakly turbulent regimes, and quasilinear stabilization. We summarize some of the literature on these processes in an infinite plasma.

4.3.1.2 Beam Trapping

As a simple example consider a 1-D beam excited spectrum which might be excited, for example, by a cold beam in a plasma in a strong magnetic field, in which $\omega_{pe} << \Omega_e$, where ω_{pe} is the plasma frequency and Ω_e is the electron cyclotron frequency. Unstable modes with wavevectors only along the beam direction of motion have to be considered. The maximum growth rate for the Cerenkov instability is $\delta_{max} \sim (n_b/2n_e)^{1/3}\omega_{pe}$, which peaks at $k_{zo} = \omega_{pe}/v_b$ with a half width given by $\Delta k_z \sim (n_b/n_e)^{1/3}k_{zo}$. As the wave exponentiates, the half width after N-foldings ($N = \delta_{max}t$) actually narrows to $\Delta k_z(N) \sim N^{-1/2}(n_b/n_e)^{1/3}k_{zo}$, so that in the limit $(n_b/n_e) << 1$ and $N >> 1$, the spectrum is quite narrow and the electric field is nearly a purely sinusoidal wave. A model proposed by W. E. Drummond et al., in Ref. 29, and computed in detail by T. M. O'Neil et al., in Ref. 30, describes trapping of the beam electrons by the monochromatic unstable electrostatic wave potential. As the wave grows, it reaches an amplitude large enough to reverse the direction of the beam trajectory. The sign of the energy exchange between the beam and the wave reverses, and the beam instability is stabilized. The wave saturation amplitude at which this occurs is given by

$$\frac{W_p}{n_b E_b} = \frac{E^2}{8\pi n_b E_b} \sim \frac{1}{2}\left(\frac{n_b}{2n_e}\right)^{1/3} \tag{17}$$

where W_p is the energy density in the wave spectrum, and n_b and E_b are the beam density and energy. The trapping velocity of the beam electrons at saturation is $\Delta v_b \sim (n_b/n_e)^{1/3} v_b$. The initial growth and saturation is rapid, occurring typically on the time scale of a few growth times, as shown in Figure 9 from Ref. 3. A numerical example of beam trapping using a computer simulation was given in S. Kainer et al., Ref. 31.

4.3.1.3 Nonlinear Stabilization

For the electron beam-plasma example above, the rapid growth and saturation of the primary excited spectrum is followed by a stage in which the primary spectrum at k_{zo} gives rise to secondary waves. An example is the sideband instability, Ref. 32, although other nonlinear processes quickly become dominant. The physical nature of the nonlinear interaction is determined by the saturation level of the primary spectrum W_p in comparison with the quantity $(k_{zo}\lambda_{De})^2$, which is a measure of the thermal dispersion of the wave. (Here λ_{De} is the Debye length, and k_{zo} is the wavenumber of the primary wave). If $(W_p/n_e T_e) < (k_{zo}\lambda_{De})^2$, the system develops by processes which can be described by weak turbulence theory, such as processes in which waves interact with particles and other waves but retain their essentially linear mode character. When

$$\left(\frac{W_p}{n_e T_e}\right) > (k_{zo}\lambda_{De})^2 \quad , \tag{18}$$

the nonlinear correction to the frequency of plasma Langmuir waves is greater than the thermal correction and the concepts of weak turbulence are no longer applicable. We first discuss some work on nonlinear stabilization, since this seems the more relevant for Schumacher's experiment, and then discuss briefly some weak turbulent processes. A good review of beam stabilization is found in the review by R. N. Sudan in Ref. 3.

a. Strong Turbulence Processes

The following discussion is for the strongly turbulent nonlinear development of the Cerenkov unstable ω_{pe} primary spectrum. For a sufficiently narrow Δk_z satisfying $\Delta k_z v_b/\omega_{pe} << 1$, the primary spectrum can be described as

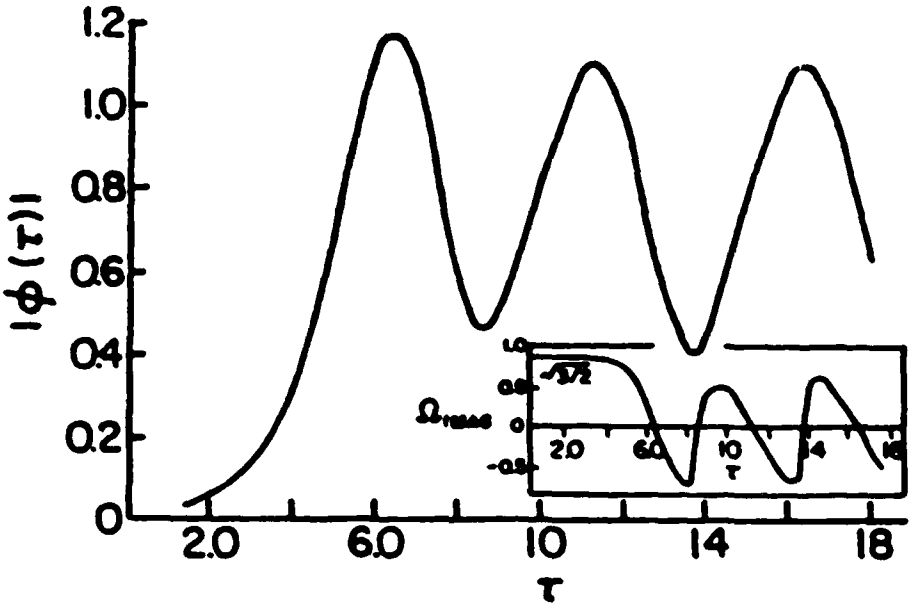

Figure 9. Plot of $\phi(\tau)$ and $\tilde{\Omega}_I(\tau)$ from numerical solution of O'Neil et al. (1971). (From Ref. 3)

monochromatic pump wave at a frequency close to ω_{pe}, which can drive other modes unstable through a parametric instability. In an infinite, homogeneous plasma, at least, the pump can couple the high and low frequency oscillations (electron plasma waves and ion acoustic waves) which exist in the plasma in the absence of the pump. Some of the various instabilities which can result are the OTSI (oscillating two-stream instability) or the modulational instability, in which a high frequency electron fluctuation at $\omega \sim \omega_{pe}$ and a purely growing ion oscillation are driven unstable, and the decay instability, when high frequency electron oscillations and low frequency ion-acoustic oscillations are driven unstable. The modulational instability represents a catastrophic growth of the initial wave modulation. This occurs in the regime in which the wavenumber of the low frequency response κ is << the pump wavenumber k_{zo}. For short waves, $(k_{zo}\lambda_{De})^2 > m_e/m_i$, the maximum growth rate of the modulational instability is

$$\delta_{max}^{mod} \sim \omega_{pi} \left(\frac{W_p}{3n_e T_e}\right)^{1/2} \tag{19}$$

for $(W_p/n_e T_e) > m_e/m_i$. The decay instability competes with the modulational instability for short wavelength waves when $\kappa \sim k_{zo}$. It has a growth rate near the three wave resonance surface of

$$\delta_{Dec} \sim \left(\frac{\omega_{pe}}{8} \kappa c_s \frac{W_p}{n_e T_e} \cos\theta\right)^{1/2} ,$$

where $\cos\theta = \underset{\sim}{k}_{zo} \cdot (\underset{\sim}{k}_{zo} + \underset{\sim}{\kappa})/|\underset{\sim}{k}_{zo}||\underset{\sim}{k}_{zo} + \underset{\sim}{\kappa}|$. A recent review which covers the development of Langmuir plasma turbulence is given by V. E. Zakharov in Ref. 34.

The Zakharov equations, or the nonlinear Schroedinger equation, provide a self-consistent model for these parametric instabilities. Besides describing the modulational and the decay instabilities, the nonlinear development of these equations can lead to the phenomenon of Langmuir wave collapse, or condensate instability. This can occur for $\kappa >> k_{zo}$, and is similar in respects to the modulational instability. The region corresponding to the different types of monochromatic wave instabilities is shown in Figure 10,

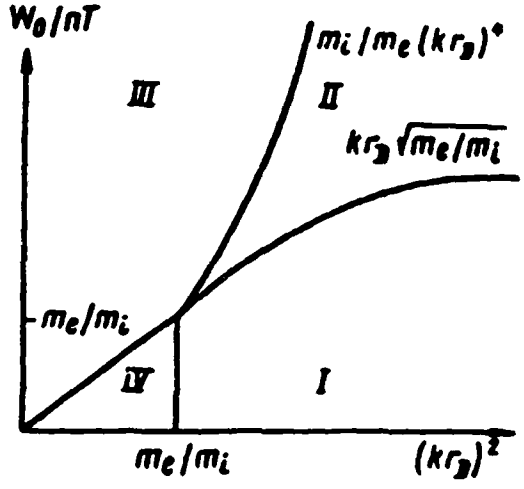

Figure 10. Location of different instability types for monochromatic Langmuir wave in plasma without magnetic field: (I) modulational instability; (II) modified decay instability; (III) uniform field instability; (IV) decay instability + modulational instability (at $T_i \ll T_e$), induced scattering + modulational instability (at $T_i \sim T_e$). (From Ref. 34)

taken from Zakharov's review in Ref. 34. Other reviews and papers relating particularly to the role of strong turbulence in the stabilization of the electron beam-plasma Cerenkov instability are given in Refs. 35-39.

In the paper by Papadopoulos, Ref. 36, there is a graph of the regions in parameter space in which either nonlinear or quasilinear stabilization occurs for a non-relativistic, collisionless plasma: this is given in Figure 11. We note that even though Schumacher and Santoru's experiments may fall in the regime of nonlinear stabilization, collisions may be important; the implications of this will be discussed in the application section. The stabilization of the electron beam-plasma interaction by strongly turbulent processes was studied analytically and numerically for a wide range of collisionless plasma parameters in the paper by Freund et al. in Ref. 35. This paper confirms some scaling laws between beam-plasma instability growth rates and electrostatic field fluctuations given in an earlier paper by Papadopoulos et al. in Ref. 37.

Because collisions between electrons and neutrals and ion charge exchange collisions are both significant for the parameter regimes of Schumacher's experiment, the most relevant references on these nonlinear parametric instabilities are those that include the effects of electron and ion collisions. There has been recent work on the modulational instability, the decay instability, and solitons within the context of a theoretical description of ionospheric heating experiments. This is one parameter regime in which collisions can be important in the sense that the collision frequency can be a significant fraction of the instability growth rate. A paper by G. L. Payne et al., Ref. 40, shows that both the OTSI and the PDI have lowered growth rates when the ion damping is large, but the OTSI is less affected (Figure 12 from Ref. 40). This is presumably because the modulational instability doesn't oscillate, and has only its growth resisted by damping, while the decay products of the PDI have both their oscillation and growth resisted by damping. Electron collisions compete directly with the growth rate of these instabilities, that is, the electron collision frequency essentially is subtracted from the instability growth rate to get the effective growth of these instabilities. As such, the growth of the modulational instability, for example, has to be > the electron collision frequency in order for it to be

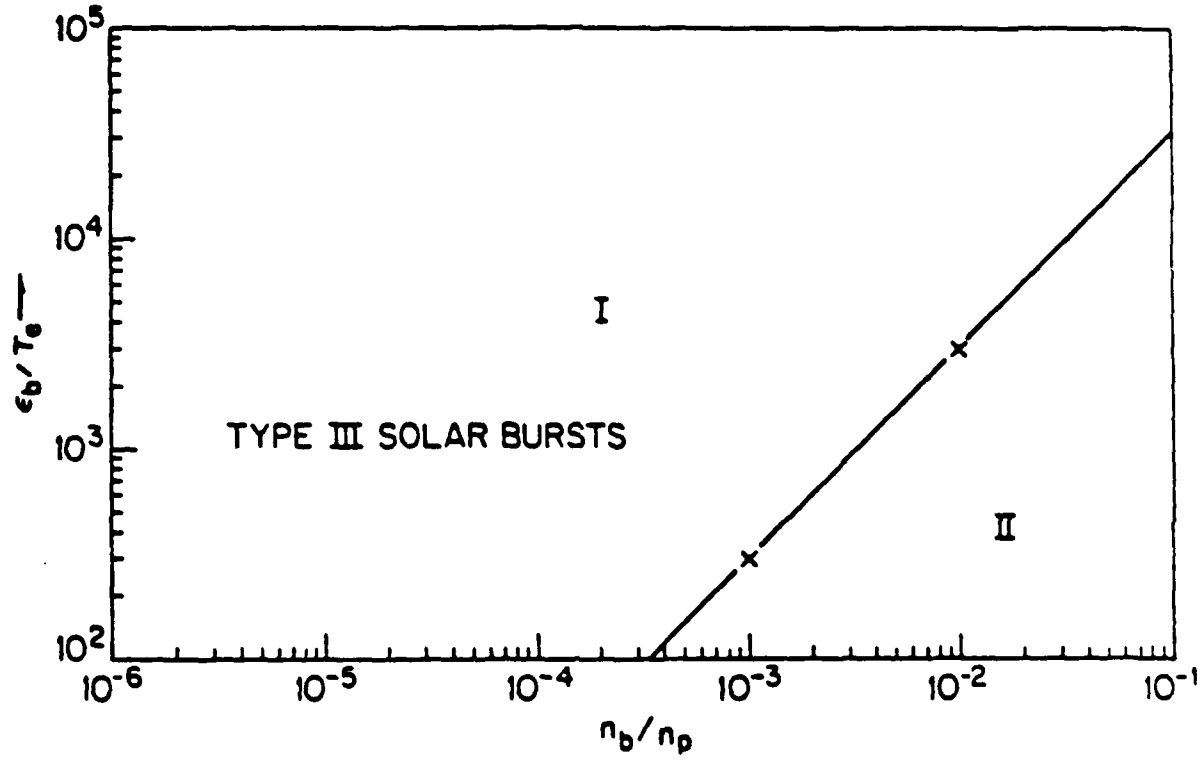

Figure 11. Regions in parameter space where nonlinear stabilization (I) and quasilinear stabilization (II) occurs for a nonrelativistic plasma. (From Ref. 36)

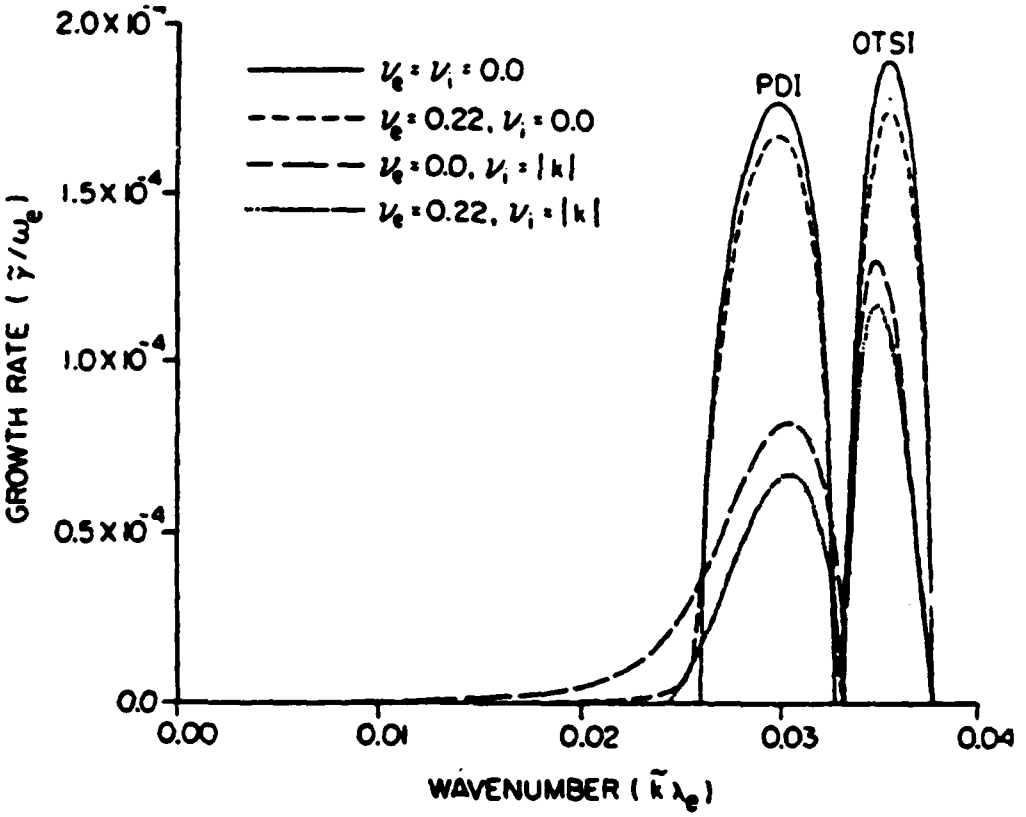

Figure 12. Positive growth rates for the linearized Zakharov equations as a function of the wave number, $\tilde{k}$, for various values of the damping coefficients. Since the dispersion equation is an even function of $\tilde{k}$, only the growth rates for positive values of $\tilde{k}$ are shown. The portion of the curves marked OTSI corresponds to the oscillating two-stream instability which is a purely growing mode for all four cases. The portion marked PDI corresponds to the parametric decay instability which has a nonzero value for the real part of the frequency ω. Note that the various curves have been labeled by the dimensionless values of the damping coefficients. (From Ref. 40)

able to stabilize the beam. Reference 40 also follows numerically the nonlinear evolution of the modulational instability, using Zakharov's equations. After an initial transient stage, the Langmuir waves become intense enough to collapse into soliton-like structures, with a spatial width related to the wavelength of the modulational instability. Other related papers on the role of these kinds of instabilities in ionospheric heating experiments include Refs. 41 and 42.

There have also been papers on the role of strong turbulence in type III solar radio bursts. Type III solar radio bursts are thought to be associated with an intense level of electron beam excited Langmuir waves, which can scatter off of or couple with other waves to produce observed electromagnetic radiation at the local plasma frequency and its second harmonic. The stabilization of these electron beams, which are emitted at the sun's surface and may propagate to the earth's orbit and beyond, may also occur by the nonlinear parametric instabilities involving strong Langmuir turbulence. In D. R. Nicholson et al., Ref. 43, and M. L. Goldstein et al., Ref. 44, the OTSI and related instabilities were applied to the stabilization of these electron beams. In this parameter regime, ion collisions, at least, had to be retained in the analyses.

Some numerical experiments, or computer simulations, have shown that strong turbulence processes, in the appropriate parameter regimes, stabilize the beam-plasma instability before quasilinear plateau formation. These include Refs. 45 and 31. Collisions were not included in the simulations, and these are probably quite important in analyzing Schumacher and Santoru's mm wave experiment. (We understand that it is quite difficult to include collisions in a simulation, Ref. 33).

b. Weak Turbulence Processes

If the energy density of the beam excited Langmuir waves is such that $W_p/n_eT_e < (k_{z0}\lambda_{De})^2$, or if strongly turbulent processes are quenched due to collisions, for example, then various nonlinear processes within weak turbulence theory can contribute to beam stabilization. One such process is the merging of two electrostatic ω_{pe} waves into a transverse wave with frequency $\omega = 2\omega_{pe}$. However, the reciprocal value of the typical time of this process,

$$\frac{1}{\tau} \sim \omega_{pe} \left(\frac{W_p}{n_e T_e}\right) \left(\frac{v_{Te}}{c}\right)^2 \quad , \tag{20}$$

is generally quite small, unless the plasma is very hot, with v_{Te} near c. Another nonlinear process is the merging of one Langmuir wave and one transverse wave into a transverse wave. The inverse of the typical time of this process is

$$\frac{1}{\tau} \sim \omega_{pe} \left(\frac{W_T}{n_e T_e}\right) \left(\frac{v_{Te}}{c}\right)^2 \quad , \tag{21}$$

where W_T is the energy density of initial transverse waves. This inverse time scale could be large if there was an intense bath of transverse waves present. Other processes include the Thompson or Compton scattering of Langmuir waves on electrons and ions. All of these weak turbulent processes are discussed and referenced in the review by Sudan in Ref. 3.

4.3.1.4 Quasilinear Stabilization

The quasilinear approximation is suitable for bump-in-tail distributions but its validity for highly energetic $v_b >> v_{Te}$, cold $\Delta v_b/v_b << 1$, beam-plasma interactions is limited. (Here v_b is the beam directed speed, v_{Te} is the electron background thermal speed, and Δv_b is the electron beam thermal speed.) Aronov (a), Ref. 9, nevertheless, considered the quasilinear relaxation of a beam in a plasma-filled waveguide. The spectrum of unstable modes is anisotropic, with a very broad spectrum in $k_\perp$. Quasilinear relaxation of the hydrodynamic beam-plasma instability would be possible if either

$$\delta < k_z(\Delta v_{b\parallel}) \qquad \text{or} \qquad \delta < k_\perp(\Delta v_{b\perp}) \tag{22}$$

for the lowest order radial mode with $k_{\perp min} = 2.4/r_g$. (Here δ is the growth rate, $\Delta v_{b\parallel}$ and $\Delta v_{b\perp}$ are the axial and perpendicular beam electron thermal spreads, and r_g is the waveguide radius.) For non-relativistic beams, under the dense plasma condition $\omega_{pe}^2 >> (2.4\ v_b/r_g)^2$, Aronov (a) found the beam

relaxation to be nearly one-dimensional, along the beam direction (axial), and accompanied by preferential increase of longitudinal beam heating ($T_{b\parallel} >> T_{b\perp}$). The level of Langmuir turbulence was found to be of the order of 1/2 $(n_b/2n_e)^{1/3}$, which is essentially the same as the beam trapping result.

An interesting, albeit very early paper, by Fainberg et al., Ref. 47, shows that when an electron beam is continuously injected into a bounded plasma, the total energy density of the excited waves can be greater than the single shot case. This is because the excitation of waves takes place continuously as new fast beam electrons are injected into the plasma. If the energy transport velocity of the waves, viz., the group velocity, v_g, is much less than the velocity of the beam electrons, v_b, then the excited waves accumulate near the beam front. The energy density in the plasma waves can be greater than the beam energy density by a factor (v_b/v_g).

4.3.2 Application to mm Wave Experiment

4.3.2.1 Beam Trapping and Quasilinear Stabilization

The Cerenkov beam-plasma instability in Schumacher's experiment appears to be in the hydrodynamic regime, because the beam thermal spread $\Delta v_b/v_b$ is less than $(n_b/n_e)^{1/3}$. As such, the Cerenkov instability is strong, with growth rate $\propto (n_b/n_e)^{1/3}\omega_{pe}$, and one would expect a high level of unstable waves. The spectrum is probably broad in $k_\perp$, as discussed in the section on beam-plasma instability, while the spectrum in k_z is narrow, of the order of $\sim (n_b/n_e)^{1/3} N^{-1/2}k_{zo}$, after N foldings. One might expect beam trapping in the longitudinal direction, because the spectrum is quite narrow in k_z, and quasilinear relaxation in the transverse direction, because the spectrum is broad in $k_\perp$. However, even though the spectrum is broad in $k_\perp$, it is quantized according to the condition $J_m(k_{\perp mn}r_g) = 0$. If only a few modes are excited (higher order modes being damped by beam thermal effects), the situation is more like beam trapping.

What are the relative magnitudes of the axial electric field E_z and the perpendicular, or radial, electric field E_r for the beam excited axisymmetric modes? The axial field is related to the perpendicular field by

$E_z \approx (k_z/k_\perp)E_r$. For the lowest order mode, $k_\perp = 2.4/r_g \sim 1.26$ cm^{-1}, and thus $E_z \sim 7E_r$ for the standard case. However, for a higher order mode, such as the axisymmetric mode with 3 radial nodes, $k_\perp \sim 4.5$ cm^{-1}, and $E_z \sim 2E_r$. Thus it appears that the perpendicular electric field could play a significant role in the wave-particle interactions for higher order modes, at least.

However, let's assume that the beam does trap in the longitudinal direction and see what follows from this. The beam would trap in the potential of the unstable ω_{pe} waves on a short time scale, of the order of a few growth times. The saturation energy density of the unstable waves is of the order of $W_p/n_bE_b \sim 1/2(n_b/2n_e)^{1/3}$. If we assume that the initial level of waves is the thermal level, $W_p/n_eT_e \sim 1/2\ \pi n_e\lambda_{De}^3$, where λ_{De} is the electron Debye length, then it would take a time

$$t \sim \frac{1}{\delta_{max}} \ln \left[\frac{1}{2}\left(\frac{n_b}{2n_e}\right)^{1/3} 2\pi n_e\lambda_{De}^3\right] \tag{23}$$

to reach the saturation level, assuming the energy grows as $\exp(\delta_{max}t)$, and that $n_eT_e \sim n_bE_b$. Using the standard case parameters, this is of the order of 6-7 growth times, with the growth time $\delta^{-1} \sim (0.07\ \omega_{pe})^{-1}$, which is about 1.2-1.4 ns. The saturation level for the standard case is of the order of $(W_p/n_bE_b) \sim 0.03$. (During this time, a beam of directed energy E ~ 30 keV would have travelled about 12-14 cm, or almost the entire length of the drift tube.)

Since the perpendicular energy distribution of the beam is like a bump-on-tail, that is, $T_{b\perp} > T_{e\perp}$, we might speculate that the beam undergoes quasilinear relaxation in the perpendicular direction, while being trapped by the potential associated with E_z in the longitudinal direction. In Aronov (a), Ref. 9, a quasilinear analysis was done for beam saturation in a plasma-filled waveguide. Using their expressions, with standard case parameters: the saturation energy of the axisymmetric, lowest order mode is $(W_p/n_bE_b) \approx 1/2\ (n_b/2n_e)^{1/3}$, same as the beam trapping value; the longitudinal beam temperature is increased preferentially over the perpendicular temperature, with $T_{bz}^{max} \sim (n_b/2n_e)^{2/3}\ m_ev_b^2 \sim 270$ eV, and $T_{b\perp}^{max} \sim (k_\perp^2/2k_z^2)\ T_{bz}^{max} \sim 2.6$ eV. We note that this small value for $T_{b\perp}$ is consistent with a low perpendicular thermal beam pressure needed for the Bennett pinch.

4.3.2.2 Nonlinear Stabilization

a. Strongly Turbulent Processes

Using the value estimated above for the energy density of the unstable ω_{pe} waves, we can estimate whether this is large enough to be in the strongly turbulent regime. The quantity $(k_{zo}\lambda_{De})^2$ is of the order of (T_e/E_b) for the Cerenkov unstable waves. For the standard case, this quantity is of the order of 2×10^{-4}. Then the conditions for strong turbulence to be present, $W_p/n_e T_e > (k_{zo}\lambda_{De})^2$, is satisfied.

However, electron-neutral, electron-ion, and ion charge exchange collisions can be significant in this experiment, and can affect the development of strongly turbulent stabilization processes. In the application section on beam focusing we estimated the electron-neutral collision frequency to be of the order of $\nu_{en} \sim 10^8\ s^{-1}$ for the standard case, and the electron-ion collision frequency was estimated to be of the order of $\nu_{ei} \sim 10^7\ s^{-1}$. The ions also suffer charge exchange collisions, with the resonant charge exchange cross section for He^+ in He given by the graph in Figure 13 taken from Ref. 8: for the standard case, $\nu_{in} \sim 10^6\ s^{-1}$.

How will the electron and ion collisions affect the growth rate of the modulational and related instabilities in this case? Following Papadopoulos, Ref. 37, and Sudan, Ref. 3, we write the Zakharov equations in the approximate but more physically transparent form in terms of the energy density of waves in the primary ω_{pe} spectrum, W_p, in the secondary spectrum W_s^e, and in the ion fluctuations W_s^i of the secondary spectrum:

$$\frac{1}{2}\frac{d}{dt} W_p = \delta_p W_p - \delta_s(W_p)\, W_s^e$$

$$\frac{1}{2}\frac{d}{dt} W_s^e = (\delta_s - \Gamma_s^e)\, W_s^e$$

$$\frac{1}{2}\frac{d}{dt} W_s^i = (\delta_s - \Gamma_s^i)\, W_s^i \quad . \tag{24}$$

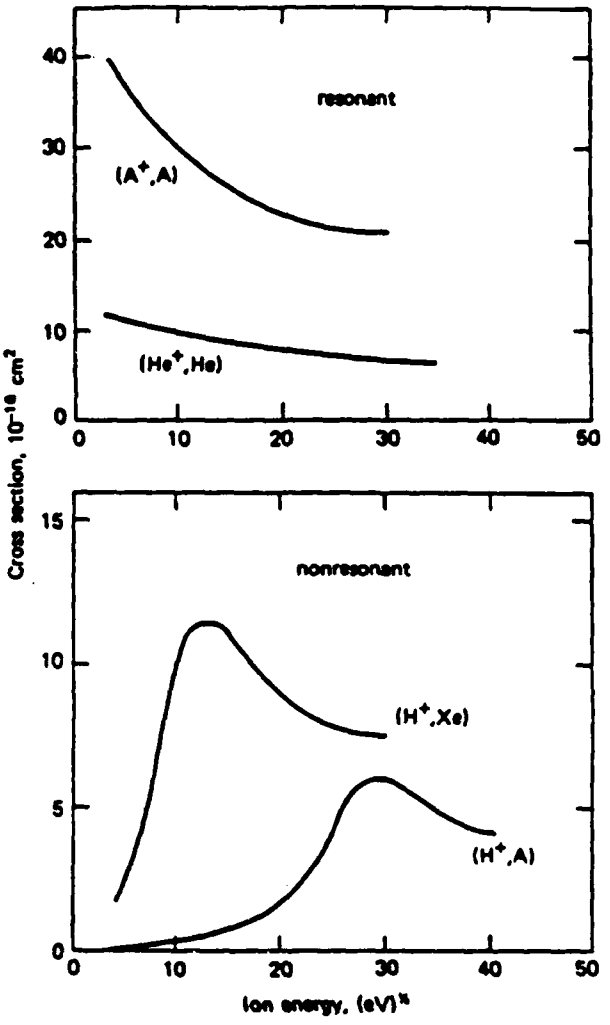

Figure 13. Charge transfer (charge exchange) cross sections. Resonant charge transfer for A^+ in argon and He^+ in helium, and nonresonant charge transfer for H^+ in xenon and H^+ in argon (after Hasted, 1951; and Massey and Burhop, 1952, p. 529). (From Ref. 8)

Here δ_p is the mean linear growth rate of the primary waves, $\delta_s(W_p)$ is the rate at which the secondary spectrum is generated by nonlinear interaction, and Γ_s^e and Γ_s^i are the mean damping rates of the secondary waves and the ion fluctuations, respectively. (We neglect electron Landau damping because the primary unstable wavenumber $k_z \sim (\omega_{pe}/v_b)$ would have to increase to $k_z \sim \lambda_{De}^{-1}$ in order for this to be important; and we neglect ion Landau damping because $T_e >> T_i$ in this experiment.) For the modulational instability in the regime $(W_p/n_eT_e) > (k_z\lambda_{De})^2 > m_e/m_i$, the maximum growth rate is given by Eq. (19) as

$$\delta_s = \delta_{MOD}^{max}(W_p) \sim \omega_{pi}\left(\frac{W_p}{3n_eT_e}\right)^{1/2} ,$$

where ω_{pi} is the ion plasma frequency. In order for the modulational instability to go, δ_{MOD} has to be greater than the damping rate Γ_s^e. For $\Gamma_s^e \sim \nu_{en} \sim 10^8\ s^{-1}$ for the standard case, then $\delta_{MOD} > \Gamma_s^e$ would imply that (W_p/n_eT_e) has to be > 0.04. Using standard case parameters, $(W/n_eT_e) \sim 0.09$ from beam trapping, so that the modulational instability could go with $\delta_{MOD}^{max} \sim 1.5\ \nu_{en}$. In actuality, δ_{MOD} should be a few times larger than the damping rates in order for the nonlinear evolution to proceed. It seems possible that electron collisions could prevent the growth of the modulational instability in this experiment in some regimes, or at least, reduce its growth. We note that as n_e decreases, it is harder to satisfy $\delta_{MOD} > \nu_{en}$. We note also that the growth of the modulational instability scales as $m_i^{-1/2}$. If the standard case parameters were held constant, but the ion mass increased by switching to Xe gas, for example, then $\delta_{MOD}^{max} \sim 0.08\ \nu_{en}$ and the modulational instability would be quenched. Because the ion collision frequency is so low in the standard case, $\nu_{in} \sim 10^6\ s^{-1}$, compared to $\nu_{en} \sim 10^8\ s^{-1}$, ion collisions may not be important in determining the effective growth rate of the instability, rather only its character, i.e., OTSI versus PDI.

It appears in this experiment that, at least in the present parameter regimes, (1) the modulational instability may not develop, or may develop only with a reduced growth rate, and (2) the waves which interact to produce the $2\omega_{pe}$ radiation are those from the primary beam-unstable spectrum, and not from a secondary spectrum which would result from the nonlinear development of a

modulational instability. In support of (1), we note that the growth rate for the modulational instability (probably the PDI has a lower growth rate because ion-acoustic oscillations are damped, that is, $\nu_{in} \sim k_z c_s$, for $k_z \sim \omega_{pe}/v_b$) is of the order of $\delta_{MOD}^{max} \sim \omega_{pi} (W_p/3n_eT_e)^{1/2}$. Now $(\omega_{pi}/\nu_{en}) \sim 9$ for the standard case. But as the ion mass increases, with pressure held constant, ω_{pi} decreases while ν_{en} increases. For example, for a background argon gas, with standard case parameters, $\nu_{en} \sim 3.6 \times 10^8$, while $\omega_{pi} \sim 3 \times 10^8$. In this case, (W/n_eT_e) would have to be ~ 1 in order for the modulational instability to go. This is a very large value, of course, but it might be possible if (n_b/n_e) increases substantially due to beam focusing. In support of (2), the experimental data indicates that the beam energies of the two beams have to be very close, at least at the lower energies and currents, in order to get maximum radiation output at $2\omega_{pe}$. Since $\omega \approx k_z v_b$, then $k_z \sim \omega_{pe}/v_b$ for the maximally growing modes. For $v_b < c$, $k_p > k_T$, where k_p and k_T are the electrostatic and electromagnetic wavenumbers, respectively: so in order to satisfy momentum conservation for the three-wave process (see section on radiation mechanisms), $\underset{\sim}{k}_{p2} \approx -\underset{\sim}{k}_{p1}$. This is precisely the relation between the wavenumbers of the beam excited modes when the beams have near equal, but oppositely directed, energies. As the energies of the beams increase, so that $v_b \sim c$, then it's not necessary to have matching because the phase velocities of the beam excited modes are near c. If the radiation at $2\omega_{pe}$ were produced by the coalescence of waves of the secondary spectrum which developed nonlinearly in the strongly turbulent regime, then one would expect that the dependence on the beam energies would be washed out. This is because the k_s of the secondary spectrum would depend on the nonlinear development of the modulational or related instabilities, and not on the beam energies. Another point is that radiation at $2\omega_{pe}$ is modulated on the time scale of the ion plasma frequency. This time scale is of the order of the growth time of the modulational instability for $(W_p/n_eT_e) \sim 1$. If the modulation of the radiation is due to a beam relaxation process, then there wouldn't be enough time for the modulational instability to develop nonlinearly. One more point to support (2) indirectly is that it appears that we can get ball park agreement with the radiation power using weak turbulence estimates, with (W_p/n_eT_e) given by beam trapping saturation values. This will be shown in the section on radiation mechanisms.

We note that it may not be good to have modulational instabilities. Since the modulational and related instabilities can stabilize the beam at lower wave saturation levels than is required by beam trapping or quasilinear theory, it may be better to stay out of this regime. Tuning of the radiation would appear to be better accomplished if the beams were stabilized by trapping. Then monochromatic waves with narrow wavebands would interact. A trade off exists however; if the modulational instability develops into solitons or cavitons, the energy density of the secondary waves could be quite large because the volume in which the waves are trapped is small, of the order of a few λ_{De} for each soliton.

One possible way to determine if soliton turbulence exists might be to see if the electron beam is scattered by the turbulence, Ref. 3. If the Langmuir wave energy W_p/n_eT_e collapses into N blobs or cavitons per unit volume, of typical size a few Debye lengths, then a beam of electrons can be strongly scattered by these blobs. If successive interactions with the blobs are random in character, then the typical time τ_D for diffusing through a radian for the beam electrons scales as

$$\tau_D \sim \frac{\omega_{pe}}{\gamma_b} \left(\frac{W_p}{n_eT_e}\right)\left(\frac{T_e}{E_b}\right)^{3/2} . \qquad (25)$$

For Schumacher's experiment, this time scale is much longer than the time it would take a beam electron to traverse the length of the device with it's original energy. For the standard case with $(W_p/n_eT_e) \sim 1$, this time scale is ~ 5 μs, while the time for a beam electron with 30 keV to transit the length of the device is of the order of 2 ns. This is probably not a viable test for this short device.

b. Weak Turbulence Processes

What about the role of weak turbulence nonlinear processes in beam stabilization? The three-wave interaction in which two longitudinal ω_{pe} waves coalesce into a transverse wave at $2\omega_{pe}$ occurs on a time scale $1/\tau \sim \omega_{pe}(W_p/n_eT_e)(v_{te}/c)^2$. Since $(v_{te}/c)^2 \sim 2 \times 10^{-5}$ for this experiment, this time scale is much too long (of the order of 1/2 μs for standard case parameters

with $(W/n_eT_e) \sim 1$) for this process to be important on the time scale of the modulation of the radiation. However, suppose the unstable waves really do pile up near the beam head with an energy density (v_b/v_g), Ref. 47, larger than the quasilinear saturation estimate. For an infinite plasma, $v_g \sim v_{Te}^2/v_b$, so that the time scale, using the same parameters, becomes of the order of 10^{-5} ns, which is too fast (being << the growth time of the Cerenkov beam-plasma instability), so there's a problem with this interpretation now.

4.3.2.3 Time Scale of Modulation of the Radiation

A comment about the time scale of the modulation of the $2\omega_{pe}$ radiation, and how this could be related to processes of beam stabilization. The observed time scale is of the order of the ion plasma frequency, which for a helium plasma is of the order of 0.01 ω_{pe}. Now this time scale can actually correspond to a list of different processes: (1) ω_{pi}^{-1} is of the order of the time scale for beam trapping; that is, the growth of the Cerenkov beam-plasma instability is $\delta \lesssim 0.1\ \omega_{pe}$, and the time scale for beam trapping is a few, 6-7 growth times; (2) the time scale for the growth of the filamentation instabilities is also of the order of ω_{pi}^{-1}; that is, the ratio of the Weibel to the Cerenkov instability is of the order of 0.1 for typical parameters; (3) the time for the growth of the modulational instability is of the order of ω_{pi}^{-1}, for $(W/n_eT_e) \sim 1$; (4) the time scale for the beam to traverse the entire length of the device, moving with its original energy, is of the order of 2 ns for a 30 keV beam; this time scale is $\sim \omega_{pi}^{-1}$; (5) of course, the ion plasma oscillations occur on this time scale.

4.3.2.4 Work to be done

We make some comments about some of the work needed to sort out the beam stabilization aspect of the experiment. (1) A lot of the discussion on beam stabilization assumes that the Cerenkov instabilities of the two beams don't interact. If this is not the case, then we may have to consider other types of instabilities, and thus other types of beam stabilization processes. (2) What about beam trapping? Is it possible that each beam is acted on by the total field excited by the two beams? If so, how does this affect the mechanism of energy exchange between the beam electrons and the wave, and ultimately the

beam trapping mechanism? How does the nature of convective versus absolute instability affect the stabilization? In addition, what about the anisotropy of the unstable spectrum as regards beam trapping? Since the perpendicular energy distribution of the beam is like a bump-on-tail, that is, $T_{b\perp} > T_{e\perp}$, where T_b, T_e, are the beam and electron background temperatures, it's possible that the beam could undergo quasilinear relaxation in the perpendicular direction, while being trapped by the potential associated with E_z in the longitudinal direction. Also, does a pile-up of unstable waves occur at the beam head, as shown in Ref. 47 for a steady state situation? (3) We will have to do more work to determine if and how nonlinear parametric processes associated with strong turbulence play a role in beam stabilization. We should map out the regions where the modulational instability may be quenched or reduced in strength by collisions in this experiment. In order to do this, we need to solve the Zakharov equations including electron and ion collisions. We should also include losses of waves due to the three-wave interaction. (4) We haven't even discussed the stabilization and nonlinear development of the electromagnetic filamentation instability. Even though this instability grows slower than the Cerenkov instability at ω_{pe}, do the two beams interact to alter the growth rate? It may be possible that this aperiodic instability, in which the plasma is configured into filaments, could play some role in enhancing the $2\omega_{pe}$ radiation because of the associated increase in density gradients in the plasma. Some work on the nonlinear development of filamentation instabilities was done in Refs. 48 and 49.

4.4 RADIATION MECHANISMS

4.4.1 Summary of Literature

4.4.1.1 Introduction

We will discuss processes which lead to radiation at $2\omega_{pe}$, and also processes which can produce radiation at ω_{pe}. Within each section, we'll discuss radiation processes at first within the context of weak turbulence theory, in which well defined plasma waves interact with each other or with particles, but retain their linear mode character. Because it is possible that the beam in Schumacher and Santoru's experiment could be stabilized by the modulational and related instabilities in certain parameter regimes, we'll then consider radiation mechanisms associated with such strongly turbulent effects as Langmuir collapse.

Within weak turbulence theory, the allowed radiation processes which lead to radiation at the second harmonic are: (1) the merging of two longitudinal ω_{pe} waves to a transverse wave with frequency $2\omega_{pe}$, and (2) the merging of one longitudinal and one transverse wave, each with frequency $\omega \sim \omega_{pe}$, into a transverse wave at $2\omega_{pe}$. Some processes which can lead to radiation at ω_{pe} are: (1) direct conversion of beam unstable modes into electromagnetic radiation, since these modes have a finite EM component in the waveguide, (2) scattering of longitudinal into transverse waves on density gradients, and (3) scattering of longitudinal into transverse waves by electrons and/or ions.

Within the context of strong turbulence theories, radiation at $2\omega_{pe}$ can occur by the merging of antiparallel propagating Langmuir waves trapped in solitons or cavitons. In addition, weak turbulence processes may be enhanced.

Essentially all of the references found deal with infinite plasmas. Probably most of the general formulae presented for the infinite plasma are applicable, and quantization effects arising from the waveguide can be incorporated into these general analyses.

4.4.1.2 Emission Mechanisms for $2\omega_{pe}$ Radiation

a. Weak Turbulence Theory

Various review papers and books discuss the emission probabilities for the 3-wave interaction processes which yield radiation at $2\omega_{pe}$, in the weak turbulence approximation. For example, there is Ref. 50 by V. N. Tsytovich, which has intuitive and classical derivations of the 3-wave process, and there is also the book, Ref. 51, and the review article, Ref. 52, by D. Melrose.

In the 3-wave interaction process, both energy and momentum have to be conserved. This is contained in the conservation laws

$$\omega_3 = \omega_1 + \omega_2$$

$$\underset{\sim}{k}_3 = \underset{\sim}{k}_1 + \underset{\sim}{k}_2 \quad . \tag{27}$$

It follows that when 1 and 2 refer to longitudinal ω_{pe} waves, 3 can refer to a transverse wave with frequency $2\omega_{pe}$. If one of the longitudinal waves is a slow wave, with $k_1 >> \omega_{pe}/c$, so that its phase velocity $v_{ph} << c$, then momentum conservation implies that $\underset{\sim}{k}_2 \approx -\underset{\sim}{k}_1$. The emission coefficient of a transverse wave with frequency $2\omega_{pe}$ is determined by the product of the energy densities of the longitudinal plasma waves, i.e., $(W_{k_1})(W_{k_2})$, with the values k_1 and k_2 satisfying the conservation laws.

The following is a simple approximate derivation of the three-wave emission probability, following Tsytovich, Ref. 50. The emission power is defined as the amount of energy emitted by a particle per unit time per unit wavenumber;

$$P_k = k^2 \omega_k u_k \tag{28}$$

where the emission probability $u_k = e^2 v^2/\omega_k^2$, where v is the characteristic velocity of the radiating particle and ω_k is the radiation frequency at

wavenumber k. For three waves, the interaction leads to quadropole radiation. The motion of a free electron in the electric field of two waves of wavevector $\underset{\sim}{k}_1$ and $\underset{\sim}{k}_2$ and frequency ω_1 and ω_2 is described by

$$m_e \frac{d^2\underset{\sim}{r}}{dt^2} = e\underset{\sim}{E}_1[\cos(\omega_1 t - \underset{\sim}{k}_1 \cdot \underset{\sim}{r})] + e\underset{\sim}{E}_2[\cos(\omega_2 t - \underset{\sim}{k}_2 \cdot \underset{\sim}{r})] \quad . \tag{29}$$

We linearize the equation of motion, and focus on those terms proportional to E_1E_2, which are the ones that produce electron motion which has the sum and difference frequencies $\omega_1 + \omega_2$, $\omega_1 - \omega_2$. What happens is that the electron is accelerated and decelerated and emits waves at these sum and difference frequencies. The order of magnitude of the electron velocity $\underset{\sim}{v} = d\underset{\sim}{r}/dt$ which is proportional to E_1E_2 and symmetric and ω_1,ω_2 and k_1,k_2 is

$$v = \frac{e^2}{m_e^2}\left(\frac{k_1}{\omega_1} + \frac{k_2}{\omega_2}\right)\frac{E_1E_2}{\omega_1\omega_2} \quad . \tag{30}$$

The emission probability is

$$u_k = \frac{e^6}{m_e^4}\left(\frac{k_1}{\omega_1} + \frac{k_2}{\omega_2}\right)^2 \frac{E_1^2E_2^2}{\omega_1^2\omega_2^2\omega_3^2}\left\{\frac{n_e}{k_3k_1k_2}\right\} \quad , \tag{31}$$

where the factor in the { } takes into account that all the electrons in a volume of the order of the symmetrized wavelength radiate coherently.

A more exact value for the total emission power density, $\pi(2\omega_{pe})$, for this process, which we'll refer to as $\ell + \ell \rightarrow t(2\omega_{pe})$, is (Ref. 50)

$$\pi(2\omega_{pe}) = \frac{\omega_{pe}^2}{n_e m_e c^3} \int_{\sqrt{3}\,\omega_{pe}/c}^{k_{De}} (W_{k_1})^2 \left(\frac{\omega_{pe}}{ck_1}\right)^2 dk_1 \quad . \tag{32}$$

Here the waves are assumed to be slow, with $k_1,k_2 > \omega_{pe}/c$, and W_{k_1} is the energy density of the longitudinal waves per unit k_1. Note that the largest emission power is generated when $k_1 \sim k_2 \sim \sqrt{3}\,\omega_{pe}/c$; then the result reduces to the approximate result found in Sudan, Ref. 3.

We specialize to the case of waves generated by the hydrodynamic beam-plasma instability, in which $|k_1| = |k_2| = \omega_{pe}/v_b$. Assuming a 1-D spectrum with W_p flat over $\Delta k_z \sim (k_{zo}(n_b/n_e)^{1/3})/\sqrt{N}$, where N = number of e-foldings of primary wave, then the total power density is

$$\pi(2\omega_{pe}) \sim 4\sqrt{N}\,\omega_{pe}\left(\frac{W_p}{n_b E_b}\right)^2\left(\frac{n_b}{n_e}\right)^{2/3} n_b E_b \left(\frac{v_b}{c}\right)^5 . \qquad (33)$$

For the process in which a Langmuir wave and a transverse wave merge into a transverse wave near $2\omega_{pe}$, the longitudinal wave must have a phase velocity near c to satisfy energy and momentum conservation. The power density is given approximately by

$$\pi(2\omega_{pe}) \sim \omega_{pe}\, W_T \frac{W_p}{n_e m_e c^2} \qquad (34)$$

where W_T is the energy density in the transverse waves, Ref. 3. We note from here that if the conservation laws for this process are satisfied, it might be possible to increase the power output in Schumacher and Santoru's experiment by launching a guide mode which would take the place of one of the beams.

Prasad, Ref. 57, calculates a mechanism for enhanced emission at $2\omega_{pe}$ involving the scattering of an electrostatic plasma wave on an electron density fluctuation, when the electrostatic wave is coherent. The power output is proportional to W_p^2, as in weak turbulence theory, but there is a threshhold for the process, which can occur when the energy density of the electrostatic pump waves is

$$\left(\frac{W_p}{n_e T_e}\right) \gtrsim 50\left(\frac{T_i}{T_e}\right)\frac{m_e}{m_i}\left(\frac{v_{Te}}{v_{ph}}\right)^2 \frac{\omega_{pe}}{\nu_e} \qquad (35)$$

where v_{ph} is the phase velocity of the Langmuir wave, and ν_e is the electron collision frequency.

b. Strong Turbulence Theory

Various papers purport to describe conditions under which radiation at $2\omega_{pe}$ is enhanced in the strongly turbulent regime. Kamilov et. al. in Ref. 53 show that it is possible that emission can be enhanced in the presence of strong Langmuir turbulence, when certain threshhold conditions are satisfied. Formally, one multiplies the emission probability for the process $\ell + \ell \rightarrow t(2\omega_{pe})$ by an enhancement factor which is of the order of $(n_e T_e/W_p)^{1/2}$, for $(W_p/n_e T_e) < 1$. This enhancement appears to be due to stimulated emission, but the instability can only occur if the level of the transverse waves exceeds a certain threshhold value which is $W_T \sim (v_{Te}/c)^2 W_p$, where W_p is the energy density of the Langmuir condensate.

Other possibilities for enhanced emission at $2\omega_{pe}$ in the presence of soliton collapse are described with application to solar type III radio burst parameters in Refs. 54 and 55. More recent work on soliton collapse and emission of $2\omega_{pe}$ radiation with application to these solar parameters is found in Ref. 56. The latter reference considers the emission of radiation at ω_{pe} and $2\omega_{pe}$ from beam excited strong Langmuir turbulence, for the case of low density, high velocity warm beams, in parameter regimes applicable to solar radio bursts. The quadropole emission at $\omega \sim 2\omega_{pe}$ arises from collapsing Langmuir wave packets, which contain antiparallel propagating Langmuir waves. The parameter space for Langmuir collapse and subsequent radiation is very rich, and many quite different phenomena occur under different conditions. The latter paper considers only one simple case, with parameters quite different from the mm wave experiment. But it is probably the most complete analysis done so far, and indicates the complexities involved in an analysis of radiation from Langmuir collapse.

4.4.1.3 Emission Mechanisms for ω_{pe} Radiation

a. Introduction

We summarize some work done on radiation on the fundamental plasma frequency for two main reasons. First, since the eigenmodes in the beam-plasma system in Schumacher's experiment are not purely electrostatic, there may be some emission due to the finite EM component of the wave. Secondly, it's

possible to convert a purely longitudinal wave to a transverse wave by scattering on a density gradient, and this may indirectly yield some estimate of the magnitude of such gradients in the experiment. The following discussion is within the context of weak turbulence theory.

b. Direct Conversion

Aronov (a), Ref. 9, discusses the direct conversion into electromagnetic radiation of a beam unstable mode in a waveguide. The small departure from purely electrostatic behavior of the maximally growing unstable wave is due to its magnetic field, which produces a non-vanishing Poynting flux. The Poynting flux is in the axial direction,

$$P_z = \frac{c}{4\pi} \int_0^{r_g} r dr \int_0^{2\pi} d\theta \, (\underset{\sim}{E} \times \underset{\sim}{B})_z \quad . \tag{36}$$

In Aronov (c), Ref. 11, it is shown that this flux can be associated with efficiencies of the order of 30%, for certain waves within certain waveguide and beam parameter ranges. It's not clear whether this has been achieved experimentally, however.

c. Scattering on Density Gradients

G. Benford et al, in Ref. 58, summarize the approach of Tidman et. al., in Ref. 59, to consider the emission of radiation at ω_{pe} near density gradients. An electrostatic wave passes through a density fluctuation of dimensionless magnitude Δ and spherically symmetric dimension y

$$\tilde{n}_p = n_p(r) \, (V\Delta/y^3) \exp(-x^2/y^2) \quad , \tag{37}$$

where $\tilde{n}_p$ describes a fluctuation over a volume V, with radial variable x. A perturbation analysis in the small variable $V\Delta/y^3 << 1$ yields the total EM power emitted from a number N of such exponential fluctuations, in a plasma of temperature T_e:

$$P \approx \frac{N\Delta^2 V^2 E^2 v_{Te} \omega_{pe}^4}{128\pi\beta c^4} \exp\left(\frac{-k^2 y^2}{2}\right) \quad , \tag{38}$$

where $k = \omega_{pe}/v_b$, and $\beta = v_b/c$. The exponent in Eq. (38) implies that the radiation is most efficient for wavelengths larger than y, i.e., sharp gradients are most effective.

d. Scattering by Electrons or Ions

Another process that can lead to radiation at the plasma frequency is the Thompson scattering of an ω_{pe} wave by an electron and its polarization cloud, or by an ion and its associated polarization cloud of electrons. In most cases, the scattering of Langmuir waves by an electron and its "coat" is much weaker than the scattering by the "coat" of an ion, Ref. 50. This would be the case for the parameters of Schumacher's experiment. In the scattering process, the conservation laws for the total energy and momentum of the wave and particle has to be satisfied. These conditions lead to

$$\omega - \omega' \approx (\underset{\sim}{k} - \underset{\sim}{k}') \cdot \underset{\sim}{v}_{Ti} \quad , \tag{39}$$

where the primes refer to the incident wave, and v_{Ti} is the ion thermal velocity. If the direction of the wavevector changes appreciably during the scattering, then $|\underset{\sim}{k} - \underset{\sim}{k}'|$ is comparable to the absolute magnitude k and

$$\omega - \omega' \approx k v_{Ti} \approx \omega \frac{v_{Ti}}{v_{ph}} \quad , \tag{40}$$

where v_{ph} is the phase velocity of the Langmuir wave; thus, the change in frequency is very small. This process can lead to absorption or amplification depending basically on the sign of

$$\underset{\sim}{k} - \underset{\sim}{k}' \cdot \frac{\partial f_i}{\partial \underset{\sim}{p}} \quad .$$

For a Maxwellian ion distribution, this is

$$- [\omega(k) - \omega'(k')] \frac{f_i}{T_i} \quad .$$

If in a scattering process the frequency is increased, ($\omega > \omega'$), absorption occurs, while if the frequency decreases, ($\omega < \omega'$), induced wave emission occurs and amplification is possible.

4.4.2 Application to mm Wave Experiment

4.4.2.1 Emission Mechanisms for $2\omega_{pe}$ Radiation

a. Weak Turbulence Theory

Before looking toward more exotic theories involving strong turbulence effects to explain the radiation at $2\omega_{pe}$, we first consider how well weak turbulence theory explains the emission. Indeed, we've indicated in the application section on beam stabilization that it is possible that in certain parameter regimes electron collisions could slow down or even prevent the modulational instability, and other related strongly turbulent stabilization processes, from developing. Even if the modulational instability does develop at a reduced growth rate, weak turbulence radiation processes may damp the wave energy.

In addition, it is observed experimentally that voltage tuning, in the form of $E_{b_1} \approx E_{b_2}$, is required for maximum $2\omega_{pe}$ power output, at least at the lower beam energies. This would reflect momentum conservation for the three-wave interaction. It follows from Eq. (27) that when ω_1, ω_2, are longitudinal beam slow waves, with phase velocity $v_{ph} \sim v_b < c$, and ω_3 is a transverse em mode with $v_{ph} \sim c$, then $|k_{1z}| \approx -|k_{2z}|$. This implies $|v_{b_1}| \approx |v_{b_2}|$, or voltage tuning. In this case, k_{3z} is very small, i.e., near cutoff.

Assume that there is a high level of unstable longitudinal monochromatic waves of frequency ω_{pe}, which is given by the beam trapping result as (Eq. 17)

$$W_p \sim \frac{1}{2} \left(\frac{n_b}{2n_e}\right)^{1/3} n_b E_b \quad .$$

We use the weak turbulence expression given for example in Ref. 50, for the power density of $2\omega_{pe}$ radiation due to the 3-wave interaction $\ell + \ell \rightarrow t(2\omega_{pe})$, (Eq. 33)

$$\pi(2\omega_{pe}) \sim 4\sqrt{N}\,\omega_{pe}\left(\frac{W_p}{n_b E_b}\right)^2\left(\frac{n_b}{n_e}\right)^{2/3} n_b E_b \left(\frac{v_b}{c}\right)^5 \quad .$$

Inserting the above saturation level for W_p, we find

$$\pi(2\omega_{pe}) \sim 0.6\sqrt{N}\,\omega_{pe}\left(\frac{n_b}{n_e}\right)^{4/3} n_b E_b \left(\frac{v_b}{c}\right)^5 \quad . \tag{41}$$

The power radiated $P(2\omega_{pe})$ is obtained from Eq. (41) by multiplying by the interaction volume, which we estimate to be the cross-sectional area of the beam, A_b, times the length of the device, L.

First off, we note that the power $P(2\omega_{pe})$ scales as

$$P(2\omega_{pe}) \propto n_b^{7/3} E_b^{3.5} A_b \quad . \tag{42}$$

Neglecting beam focusing effects, which we will consider below, this leads to a nonlinear dependence on the initial beam current $I_b \sim n_b$. This says that the power should scale as $I_b^{7/3}$. It appears from Schumacher and Santoru's experimental data that the scaling is much steeper with I_b, possibly reflecting the nonlinear dependence of n_b on I_b. For fixed n_b, the power should scale as $E_b^{3.5}$. This might be difficult to observe experimentally unless there is some way of determining how the effective n_b in the interaction region depends on other parameters such as I_b and even E_b itself.

The observed scaling of power with I_b may be understood within the context of weak turbulence theory if the scaling of n_b with beam current I_b, were sufficiently nonlinear. Because the beam focuses, we write the effective beam density as

$$\tilde{n}_b = n_{bo}\,(A_{bo}/\tilde{A}_b) \quad ,$$

where n_{bo} is the initial injected beam density, A_{bo} is the cross-sectional area of the beam at the entrance to the guide, and $\tilde{A}_b = \pi\tilde{r}_b^2$ is the compressed cross-

sectional area, with $\tilde{r}_b$ the compressed beam radius. We assume that each beam magnetically self focuses, which appears to be plausible from the section on beam focusing, and make the ansatz that $B_o^2 \propto I_b^2/\tilde{r}_b^2 \propto n_b T_{b\perp}$ from pressure balance for each beam. If $\tilde{r}_b^2 T_{b\perp}$ is independent of I_b, then $\tilde{n}_b \propto I_b^2$. It follows then that the power would scale as

$$P(2\omega_{pe}) \propto I_b^{4/3} \quad ,$$

which may be in closer agreement with experiment. In fact, the power scales like I_b^{5-7} experimentally for a He plasma. Below some threshhold I_b, however, the power decreases exponentially.

We make some quantitative estimates of the power emitted in $2\omega_{pe}$ radiation for the standard case using weak turbulence theory. Plugging the standard case parameters into Eq. (41), and assuming $N \sim 7$ from the section on beam trapping, yields

$$\pi(2\omega_{pe}) \sim 2 \times 10^6 \text{ erg/cm}^3\text{-s} \quad .$$

Multiplying by the volume $\pi r_g^2 L \sim 1.8 \times 10^3$ cm^3, we get for the total power $P(2\omega_{pe}) \sim 36$ Watts. We compare this result to the run shown in Figure 14 (Ref. 7). The parameters of this run are somewhat close to the standard case. The power observed was of the order of 10's of Watts, although this figure may have been revised upward recently due to better calibration of losses in the waveguides, Ref. 60. If we use the experimentally determined value of $n_b \sim 6 \times 10^9$ cm^{-3} for the highest beam current cases, with the other parameters given by the standard case, then $P(2\omega_{pe}) \sim 1$ kW, which is the same order of magnitude as the experimental value of $P(2\omega_{pe}) \leq 8$ kW.

The efficiency η is defined as

$$\eta = \frac{P(2\omega_{pe})}{P(2 \text{ beams})} \quad , \tag{43}$$

35-GHz
RADIATION

TIME, 40 ns/div

$n_e = 3.8 \times 10^{12}\ cm^{-3}$

$T_e = 5\ eV$

$I_b = 2.5\ A$

$V_b = 30\ kV$

$\frac{n_b}{n_e} \cong 2.3 \times 10^{-4}$

$\frac{W_{EPW}}{n_e T_e} \cong 7 \times 10^{-2}$

$(k_p \lambda_D)^2 \cong 8 \times 10^{-5}$

Figure 14. Output mm-wave radiation is strongly modulated on a time scale which is near the ion-plasma frequency. Experiment parameters corresponding to the observed 35-GHz radiation are listed below the oscilloscope waveform. (From Ref. 7)

where the power in the two beams is

$$P(2 \text{ beams}) \sim 2n_b E_b v_b A_b \quad , \tag{44}$$

assuming the beams have the same parameters. For the previous example of the standard case, with $P(2\omega_{pe}) \sim 36$ W, and $P(2 \text{ beams}) \sim 10^5$ W, the efficiency is 3.6×10^{-4}. The scaling of the efficiency of the mm wave output with the parameters I_b and E_b, taking beam pinching into account, is

$$\eta \propto I_b^{11/3} E_b^2 \quad .$$

Thus increasing I_b by a factor of 4, say, would increase the efficiency by a factor of ~ 160 for the same input parameters. If the beam is focused owing to its own magnetic field, then there is no additional energy spent in the compression. Even if the beam is focused due to other geometrical effects inherent in the injection process, it would be a good idea to arrange parameters such that the beam does self focus (bearing in mind that there might be limitations to how high the current should be, e.g., to avoid return currents).

Are there any other ways the emission process could proceed within the weak turbulence context, but yet be enhanced above the values calculated above? It was shown in Ref. 47 that there can be an accumulation of energy in unstable plasma waves within quasilinear beam stabilization theory, when the experimental situation corresponds to steady-state, versus one-shot injection. There it was shown that $(W_p/n_e T_e)$ could be enhanced by a factor (v_b/v_g) times the usual quasilinear asymptotic level. For a Langmuir wave in an infinite plasma, $v_g \sim v_{Te}^2/v_b$, so that this enhancement factor is $\sim (E_b/T_e)$. This is quite a large number in the mm wave experiment, of the order of $3/5 \times 10^4$, which could in principle lead to an enhancement of the order of 4×10^7 in power.

Prasad's theory, Ref. 57, appears to be similar to the weak turbulent three-wave interaction, with the specification that one of the longitudinal

waves is coherent, (i.e., produced by a strong beam-plasma instability), and the other wave, or electron density fluctuation, is thermal level. At this point we don't understand how this theory leads to enhancement of radiation over the simple weak turbulence estimate discussed above, and we'll have to contact the author to discuss this more fully.

b. Strong Turbulence Theory

The discussion in the last section shows that weak turbulence estimates lead to reasonable agreement with the magnitude of the observed power of $2\omega_{pe}$ radiation in Schumacher and Santoru's experiment. The scaling of the power with beam current may also be understood within weak turbulence theory, if the effects of magnetic self focusing are included. It appears somewhat doubtful that radiation from collapsing solitons or cavitons could play a role in the experiment. First off, the radiation is present only when there are two counterstreaming beams; if soliton collapse were important, one would expect to see radiation with only one beam present. Secondly, the growth of the modulational and related instabilities appears to be reduced by electron collisions, as shown in the application section on beam stabilization. There it was also pointed out that the $2\omega_{pe}$ radiation itself may play a part in the damping of these instabilities. We note, however, that it may not be beneficial to be in the strongly turbulent regime as regards radiation processes, because it appears to be more difficult to control the spectrum, the direction of propagation, and the bandwidth of the radiation, if the radiation originates from collapsing solitons or cavitons.

4.4.2.2 Emission Mechanisms for ω_{pe} Radiation

We estimate now the power that would be emitted at the fundamental plasma frequency. First we'll consider direct conversion, and then scattering on density gradients.

a. Direct Conversion

Direct conversion into electromagnetic radiation is possible because of the finite magnetic field of the beam excited wave in the waveguide. With the field components E_z, E_r, and B_θ, the Poynting flux can either be in the axial

direction or in the radial direction. The former flux would be largest for the higher order beam excited modes, that is, for those axisymmetric modes with lots of radial nodes, because of the relation $E_r \sim (k_\perp/k_z)E_z$, $B_\theta \propto E_r$. We estimate the Poynting flux in the axial direction arising by direct conversion from a beam-plasma instability. Assume the experiment were modified so that there was only one beam, with an output guide at the opposite end of the waveguide. Assume the length of the guide was such that the maximum build up of unstable axisymmetric waves occurred near the output end of the guide. The Poynting flux is given by (Ref. 9)

$$P_z \sim \sum_n \frac{\delta_n}{2\omega_{pe}} \mu_n^2 \frac{v_b^3}{\omega_{pe}^2} |E_{zn}|^2 J_1^2(\mu_n) \quad , \tag{45}$$

where δ_n is the linear growth rate, and other notation same as in section on beam-plasma instability. The efficiency is given by (Ref. 9)

$$\eta \sim \sum_n \frac{\delta_n}{pe} \frac{\mu_n^2}{k_z^2 r_g^2} \left(\frac{E_z^2}{4\pi n_b E_b}\right) J_1^2(\mu_n) \quad . \tag{46}$$

Using the beam trapping result to estimate $(E^2/4\pi n_b E_b)$, and the growth rate $\delta \sim (n_b/2n_e)^{1/3}\omega_{pe}$, this becomes

$$\eta \sim \sum_n \left(\frac{n_b}{2n_e}\right)^{2/3} \frac{k_{\perp n}^2}{k_z^2} J_1^2(\mu_n) \quad . \tag{47}$$

For the standard case, with $r_g \sim 1.9$ cm, $k_\perp \sim 4.5$ cm^{-1} for the TM_{03} mode: the efficiency is of the order of 10^{-4}. If we go to a higher current so that $(n_b/n_e) \sim 0.05$, and consider the TM_{05} mode, then the efficiency could increase to $\eta \sim 1\%$.

b. Conversion on Density Gradients

We use Eq. (38) to estimate the power that would be emitted near $\omega \sim \omega_{pe}$ by scattering from density gradients. In Schumacher and Santoru's experiment,

the limit of detection of mw radiation is of the order of 0.1 mWatt, and no radiation at this frequency is detected. Thus this should give some upper limit to the magnitude of density gradients in the device. From Eq. (38), the power radiated at ω_{pe} due to this process is

$$P(\omega_{pe}) \sim \frac{N\Delta^2 V^2}{32\delta_o^3} \left(\frac{E^2}{4\pi}\right) (kv_{Te}) \exp\left(-\frac{k^2 y^2}{2}\right) \quad , \tag{48}$$

with y the scale of the inhomogeneity, Δ the dimensionless magnitude of the inhomogeneity, N the number of such inhomogeneities in the volume V, δ_o the collisionless skin depth, and $k = \omega_{pe}/v_b$. Assuming $P < 0.1$ mW, and using the beam trapping estimate for $(E^2/4\pi)$, assuming $V \sim \pi \times (1/2)^2 \times 15\ cm^3 \sim 12\ cm^3$, this implies that $N\Delta^2 \exp(-40.5\ y^2(cm))$ has to be $\lesssim 10^{-8}$. If $N\Delta^2 \sim 10^{-3}$, then y would have to be $\gtrsim 0.55$ cm $\sim 2\delta_o$. For a smaller Δ, of the order of $\Delta \sim 10^{-10}$, as might be characteristic of the background plasma density, we would expect to see no radiation.

4.4.2.3 Work to be done

There appears to be good agreement between experiment and weak turbulence estimates of the scaling and magnitude of the radiation power. Even so, we should try to pin this down even further. Assured that the basic physics interpretation is correct, we can make optimization studies to find the best combination of plasma, beam, and geometrical parameters for maximum power output.

We should do more work on the production of ω_{pe} radiation by direct conversion, since some of the theoretical papers claim high efficiency for this process. Also, we should investigate the possibilities of increasing the power output in radiation by using externally launched $\omega \gtrsim \omega_{pe}$ waveguide modes to interact with the beam excited modes.

We should also investigate the role, if any, of the filamentation instability in enhancing the magnitude of the three-wave interaction owing to the density inhomogeneities created by this aperiodic instability. We should investigate the accumulation effect, i.e., the increase of W_p near the beam head in this steady injection experiment, and its effect on the radiation process.

4.5 OTHER EXPERIMENTS

In this section we'll review some beam-plasma experiments which observe radiation at $2\omega_{pe}$. We pay particular attention to the scaling of power and efficiency with (1) beam current, (2) beam energy, (3) strength of the beam-plasma interaction, and (4) energy density of the beam excited waves. In order to compare these experiments with Schumacher and Santoru's experiment, we will delineate the parameter regimes: this will also include dimensionless parameters, such as (r_b/r_g), $((r_g - r_b)/\delta_o)$, ν/δ, $(I_b/I_{Bennett})$, where δ is any growth rate of interest, and ν is a collision frequency.

Radiation at $2\omega_{pe}$ has been observed in several laboratory experiments, documented in Refs. 61-68, which we'll refer to as A - F below. Experiments A - C comprise counterstreaming electron beams in a plasma, while D - F comprise single electron beams propagating through a plasma. We briefly review the parameter regimes and results of these.

4.5.1 Experiment A

4.5.1.1 Summary of Experimental Results

The experiment of Intrator et. al., Ref. 61, was a steady-state laboratory experiment, in which counterstreaming, large diameter electron beams were injected axially into a larger cylindrical plasma-filled target chamber. The target chamber is 92 cm long by 66 cm in diameter. The radial beam density profile has a 1/e diameter of 14 cm or less in the interaction volume, and the beam radius appears to get narrower as it propagates in the target chamber. Typical background plasma parameters are of the order of $n_e \sim 10^{10}$ cm^{-3}, $T_e \sim$ 1-4 eV, $P < 2.5 \times 10^{-5}$ Torr for Ar and Xe, $(\nu_{en}/\omega_{pe}) < 10^{-1}$, and $B_{oz} < 50$ G. Typical beam parameters are $(n_b/n_e) < 10^{-2}$, and $E_b < 350$ eV. Using these parameters we have $\omega_{pe} \sim 5.6 \times 10^9$ s^{-1}, $\Omega_e \sim 10^8$ s^{-1}, $v_b \lesssim 10^9$ cm/s, and $(\Omega_e/\omega_{pe}) << 1$. The ratio $(r_b/r_g) \sim 0.4$ in the interaction region, while $\delta_o \sim$ 5.3 cm and $((r_g - r_b)/\delta_o) \sim 3.6$.

The beams excite electrostatic waves at the upper hybrid frequency, which is of the order of ω_{pe} because $(\Omega_e/\omega_{pe}) << 1$, with hydrodynamic growth rate, which for $(n_b/n_e) \sim 10^{-3}$ is $\delta \sim 0.08\ \omega_{pe}$. The electrostatic wave energy density is estimated experimentally to be $(W_p/n_eT_e) \sim 10^{-3} - 10^{-2}$. If we

compare this value with $(k_z\lambda_{De})^2 \sim T_e/E_b \sim 2/350 \sim 5.7 \times 10^{-3}$, we see that the experiment may still be in the weakly turbulent regime, with $(W_p/n_eT_e) \lesssim (k_z\lambda_{De})^2$. Actually it is curious that the electrostatic fluctuation level is so low, because beam trapping would give a saturation level of $(W_p/n_eT_e) \sim 0.02$. It would appear that some process, such as the modulational instability or the parametric decay instability, is preventing the beam saturation level from being reached. If this is so, then the growth rate for the modulational instability would be $\delta_{MOD}^{max} \sim \omega_{pi} (W_p/3n_eT_e)^{1/2}$, and for $(W_p/n_eT_e) \sim 5 \times 10^{-3}$, $\delta_{MOD}^{max} \sim 0.04\ \omega_{pi}$.

The emission at $2\omega_{pe}$ is quadropole in nature, indicating a process in which two waves with $\omega \sim \omega_{pe}$ merge into a transverse wave with $\omega \sim 2\omega_{pe}$. The radiation appears to be accompanied by low frequency fluctuations near the ion plasma frequency. It's claimed that the scaling of the EM peak frequency versus W_{UH} does not correspond to cavity modes (Figure 15). Maybe this is because the excited beam modes have eigenfunctions which evanesce away from the beam edge, which is thin compared to the cavity radius, and so the eigenfunctions are not really cavity mode eigenfunctions.

The power emitted at $2\omega_{pe}$ when there are two counterstreaming beams is larger than the incoherent sum of the power emitted at $2\omega_{pe}$ by each beam alone. The authors say that the power levels observed when two beams are present are ~ 4 - 5 orders of magnitude larger than predicted by weak turbulence theory. We note, however, that if (W_p/n_eT_e) is given by the beam trapping value, the power levels predicted by weak turbulence theory are closer to experiment.

The efficiency of radiation output at $2\omega_{pe}$ in a xenon plasma with two counterstreaming beams is estimated to be $\sim 2 \times 10^{-4}$. The scaling of $P(2\omega_{pe})$ with beam energy goes like $P(2\omega_{pe}) \propto \exp(E_b/T_e)$ (Figure 16). No evidence is seen for a lower energy threshhold or upper energy saturation limit. The bandwidth of the radiation is small, with $(\Delta\omega/\omega) \leq 0.2$ for $\omega = 2\omega_{UH}$. Increasing the ion mass of the plasma increases the efficiency of EM power production, which the authors claim should be contained in a theory for the emission process. (We note that since the electron-neutral collision cross section increases with ion mass for He, Ar, and Xe at these electron temperatures, see Figure 17, and the growth rate of the modulational

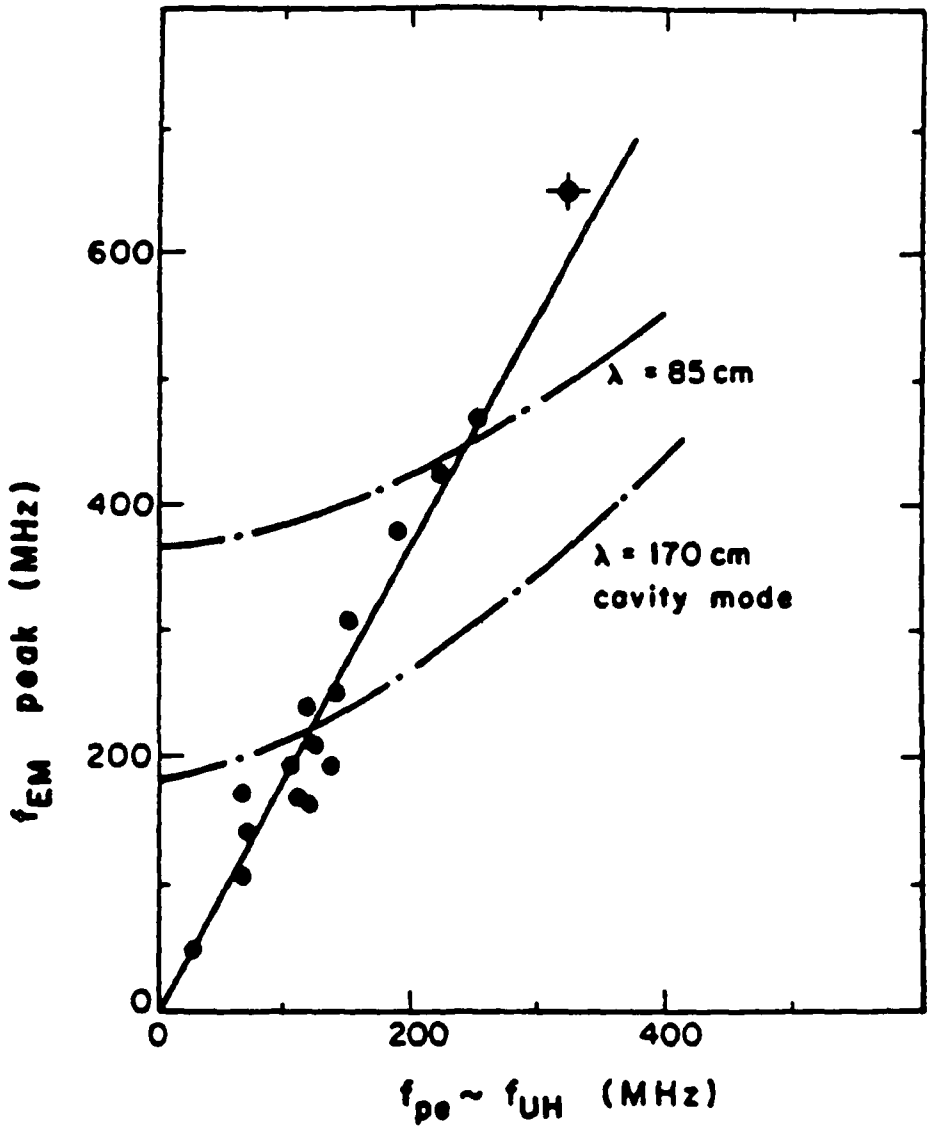

Figure 15. Graph of EM peak frequency versus the upper-hybrid frequency ω_{UH}, with best fit of $\omega_{EM} \sim 1.9 \pm 0.1\ \omega_{UH}$. (From Ref. 61)

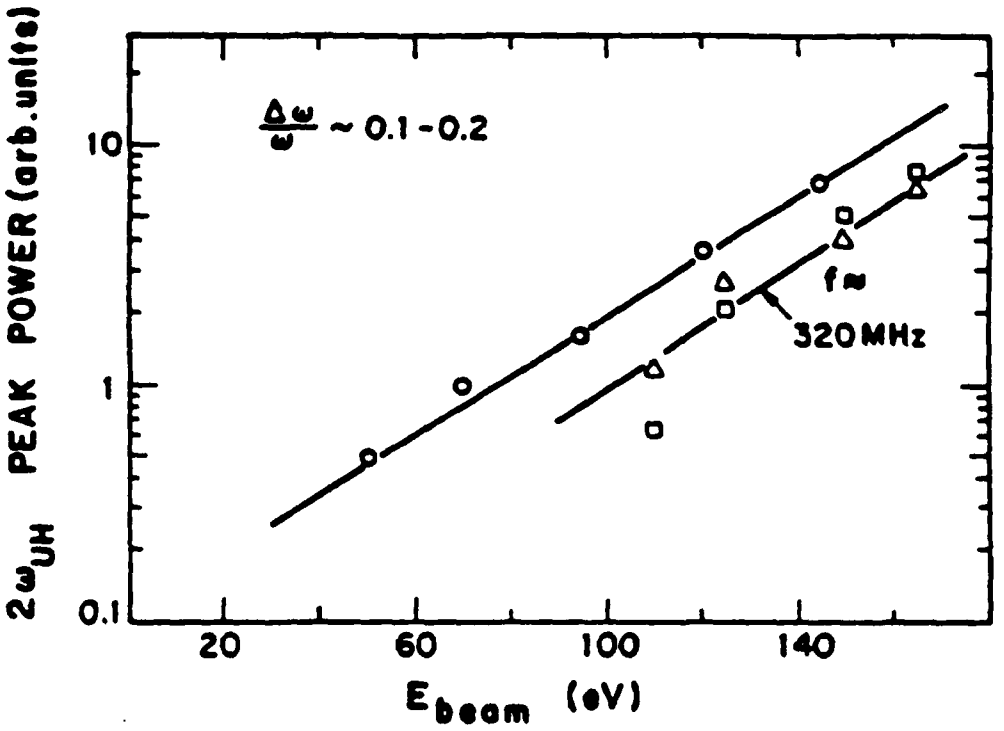

Figure 16. Graph of electromagnetic power density as a function of beam energy. The O, □, and Δ are all different data sets, and show the strongly nonlinear dependence of $\Pi_{EM}(E_b)$. (From Ref. 61)

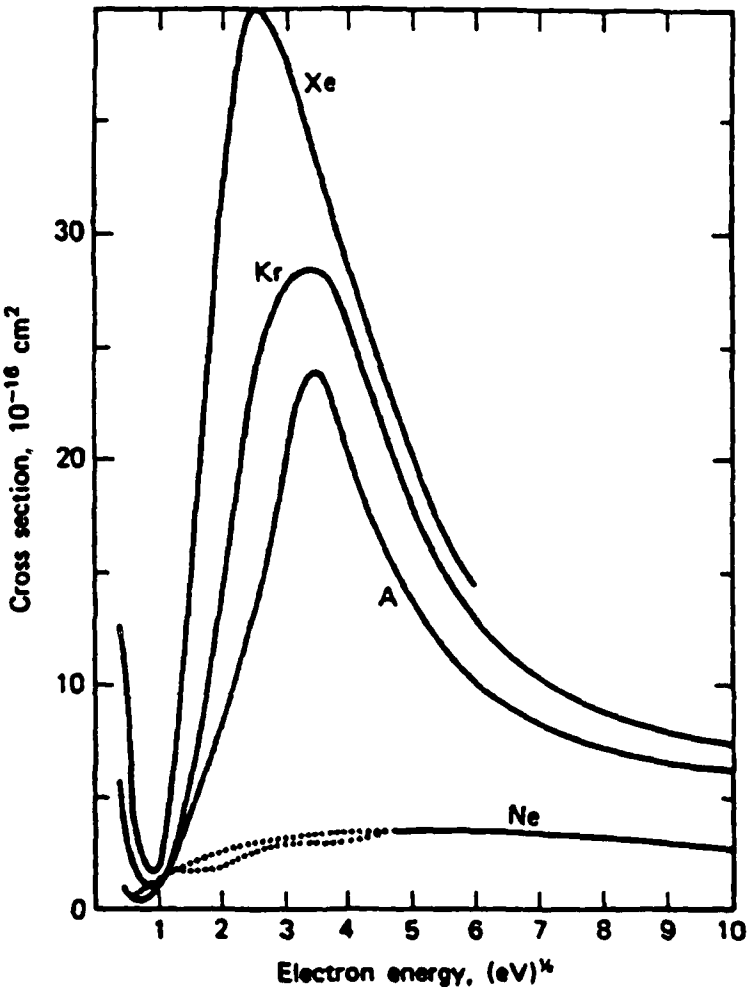

Figure 17. Total elastic collision cross sections of electrons in the noble gases Ne, A, Kr, and Xe (after Brode, 1933). (From Ref. 8)

instability decreases with ion mass, this last trend could reflect the decreased strength of the modulational instability, and possibly the concomitant increase in energy density of the electrostatic waves).

4.5.1.2 Relation to mm Wave Experiment

This experiment is similar to Schumacher and Santoru's experiment in that the radiation at $2\omega_{pe}$ comes from two counterstreaming electron beams in a plasma-filled guide, the beams being nonrelativistic and steady-state. The efficiencies are of the same order. In the Intrator et al. experiment, however, radiation at $2\omega_{pe}$ is observed from only one beam as well, while this is not the case in the mm wave experiment, at least within the detectability of the equipment, which is of the order of < 1 mwatt.

The chamber used in the Intrator et al. experiment is much larger, of the order of 6 times longer in length and 15 times wider in radius, than the mm wave experiment. The ratio of the collisionless skin depth to the chamber radius is of the order of 0.15; for a 14 cm diameter beam in the interaction region, there are about 5 collisionless skin depths between the beam edge and the conducting wall. Thus strong hydrodynamic growth of the beam-plasma instability is also to be expected in this experiment. However, because the device is so large, the beam has sufficient time to thermalize. For example, the temporal growth rate of the Cerenkov beam-plasma instability in this experiment is of the order of $0.1\ \omega_{pe} \sim 5 \times 10^{8}\ s^{-1}$, and a few growth times would be of the order of, say, 15 ns. During this time, the beam would have travelled about 10 cm with its original energy, which is only 1/10th the length of the device. In comparison, the beam in the mm wave experiment would have travelled the entire length of the device during a few growth times.

What about the modulational instability or related strong turbulence processes? First off, the parameter $(k_z\lambda_{De})^2$ is of the order of 5.7×10^{-3} in this experiment, while (W_p/n_eT_e) is estimated to be of the order of 10^{-3} - 10^{-2} from measured data; thus the condition for strong turbulence can be marginally satisfied.

We estimate the electron-neutral collision frequency in Intrator's experiment to be $\nu_{en} \lesssim 10^{5}\ s^{-1}$ for an Ar plasma at a pressure of $P \lesssim 2.5 \times 10^{-5}$ Torr, and $T_e \sim 4$ eV. The electron-ion collision frequency is of the order of 7

x 10^4. Thus collisions are unimportant relative to the plasma frequency or the growth rate of the beam-plasma instability. The growth of the modulational instability occurs at the rate $\delta_{MOD} \sim \omega_{pi} (W_p/3n_eT_e)^{1/2}$, which for $(W_p/n_eT_e) \sim 5 \times 10^{-3}$ is of the order of $\delta_{MOD} \sim 8 \times 10^5$ s^{-1}, so that the electron collision frequency is < than the growth of the modulational instability. From Figure 13 we can calculate the ion-neutral collision frequency for the Ar plasma to be about $\sim 4 \times 10^2$ for the same pressure and $(T_i/T_e) \sim 1/10$. This is different from the mm wave experiment in which both electron and ion collisions can play an important role in determining whether strong turbulence processes can develop. It appears that strong turbulent stabilization of the beam-plasma instability could be possible in the Intrator et al. experiment.

If one wanted to make more connection from the mm wave experiment to the Intrator et al. experiment, one could do a few things in the mm wave experiment. One thing would be to lower the electron neutral collision frequency relative to the modulational growth rate: this might be accomplished by going to a noble gas like A or Xe, with $T_e \sim 1$ eV in order to lower σ_{e-A}, or by going to higher plasma density and larger (n_b/n_e) so that δ_{MOD} increases. Another thing to do would be to improve the diagnostics so that a direct measure of (W_p/n_eT_e) could be made, to check the weak turbulence predictions of power radiated at $2\omega_{pe}$, as was done in the Intrator experiment. Some data manipulation which probably could be readily done would be to (1) check the scaling of $P(2\omega_{pe})$ with E_b/T_e, and (2) to retrieve a plot of frequency at peak power output versus ω_{pe}, to determine whether the emitted power follows cavity mode dispersion relations in the mm wave experiment.

4.5.2 Experiment B

5.5.2.1 Summary of Experimental Results

The experiment of Leung et al., Ref. 62, also observes $2\omega_{pe}$ radiation in a counterstreaming electron beam-plasma setup. The vacuum chamber in this case is larger than that in the Intrator et al. experiment, being 180 cm in diameter and 180 cm in length, although the background plasma density and electron temperature are similar, with $n_e \sim 10^{10}$ cm^{-3}, $T_e \sim 2$ eV, and $T_e/T_i \sim 10$. The beam densities are a bit lower than the Intrator experiment, with $(n_b/n_e) \sim 0.001 - 0.01$, and the beam energies are also lower, with $E_b \sim 100$ eV. It is

claimed that weak turbulence theory applies to this experiment: (1) the power radiated at $2\omega_{pe}$ scales as $W_p^{2\pm0.5}$, (2) the width of the electrostatic fluctuations is narrow, with $(\Delta\omega/\omega) \sim 100$ Mhz/1 Ghz ~ 0.1, which corresponds to $(\Delta\omega/\omega) \sim (n_b/2n_e)^{1/3}$ with $(n_b/n_e) \sim 0.005$, (3) the width of the peak in the $2\omega_{pe}$ radiation is correspondingly narrow, with $(\Delta\omega/\omega) \sim 300$ Mhz/2.2 Ghz ~ 0.15.

To see if the experiment is in the weakly turbulent regime we compare (W_p/n_eT_e) with $(k_z\lambda_{De})^2$. From beam trapping, $(W_p/n_eT_e) \sim (W_p/n_bE_b)\ (n_bE_b/n_eT_e) \sim (n_b/2n_e)^{1/3}\ 1/2\ (n_b/n_e)\ (E_b/T_e)$. For $(n_b/n_e) \sim 0.005$, and $E_b/T_e \sim 50$, we have $(W_p/n_eT_e) \sim 0.017$, while $(k_z\lambda_{De})^2 \sim T_e/E_b \sim 0.02$, and so it's marginal whether strong turbulence applies. We don't know what the collision frequencies are.

4.5.2.2 Relation to mm Wave Experiment

This experiment is performed in a much larger device then the mm wave experiment, so that quantization is probably much less important. Indeed, the ratio of the collisionless skin depth δ_o to the chamber radius r_g is of the order of 0.06, while the ratio of the axial wavelength of the maximally unstable mode λ_{zo} to the length of the device L is of the order of 3×10^{-3}. For comparison, in the mm wave experiment, the ratio (δ_o/r_g) is typically 0.25, while the ratio (λ_{zo}/L) is of the order of 0.03.

The ratio (n_b/n_e) is higher but the beam energy is lower than in the mm wave experiment. This latter fact means that an absolutely larger value of the ratio (W_p/n_eT_e) is needed in the Leung et al. experiment in order to put it in the strongly turbulent regime, because $(k_z\lambda_{De})^2 \sim T_e/E_b$. Whereas strong turbulence processes may not exist in the Leung et al. experiment because (W_p/n_eT_e) doesn't get large enough, strongly turbulent processes may not be able to go in Schumacher and Santoru's experiment owing to electron collisions.

To make more connection of the mm wave experiment with this other 2-beam experiment, it might be helpful to reduce the mm wave data, if possible, to (1) determine the width $(\Delta\omega/\omega)$ for the radiation, (2) do a fit to $P(2\omega_{pe})$ to see how it scales with W_p, if measurable, or with (n_b/n_e), if the effective (n_b/n_e) in the interaction region can be determined.

4.5.3 Experiment C

4.5.3.1 Summary of Experimental Results

Another counterstreaming electron beam-plasma experiment was performed by Alexeff et al., and reported in Ref. 63. In this experiment, a bumpy torus device modelled a situation in which two interpenetrating electron beams could interact with a heavy ion background. An instability at the frequency $\omega \sim (\omega_{pe}\omega_{pi})^{1/2}$ was observed, and derived theoretically. We don't see an immediate connection with the mm wave experiment right now, because the relevant instabilities in the latter experiment probably involve the interaction of the beam electrons with the background electrons.

4.5.4 Experiment D

4.5.4.1 Summary of Experimental Results

Michel et al., Ref. 64, detected both the emission of radiation at $2\omega_{pe}$ and the formation of density depressions, which they claim are consistent with the predictions of strong turbulence theory. The experiment is again steady state, and performed in a large cylindrical, plasma-filled device, with diameter 2 m, and length 3 m. The background plasma density is $n_e \sim 3 \times 10^{10}$ cm^{-3}, and the background T_e appears to be $T_e < 1$ eV. There is a weak axial magnetic guide field of $B_{oz} \sim 2 - 5$ G, so that $(\Omega_e/\omega_{pe}) \sim 7 \times 10^{-3}$. The ratio $(n_b/n_e) \sim 2 \times 10^{-3}$ for a beam diameter of 30 cm. The background gas is argon, and with $T_e \lesssim 1$ eV, and $P \sim 2 \times 10^{-4}$ Torr, the electron-neutral collision frequency $\nu_{en} \sim 4 \times 10^4$ s^{-1}. The electron-ion collision frequency appears to be $\nu_{ei} \sim 10^6$ s^{-1}.

The beam energy is varied over a wide range, from 100 eV to 5 keV. The threshhold value of beam energy for second harmonic emission was 500 eV. To see why, consider that $(k_z\lambda_{De})^2 \sim T_e/E_b$ has to be much less than (W_p/n_eT_e) in order for strong turbulence to be present. Using the beam trapping estimate, $(W_p/n_eT_e) \sim 1/2\ (n_b/2n_e)^{1/3}\ (n_b/n_e)\ (E_b/T_e)$. For $(n_b/n_e) \sim 2 \times 10^{-3}$, the condition $(W_p/n_eT_e) > (k_z\lambda_{De})^2$ implies $(T_e/E_b)^2 \lesssim 10^{-4}$. For $T_e \sim 1$ eV, this implies $E_b > 100$ eV, which is within the ball park. Actually, measurements of the density fluctuation levels and the density depressions yield $\delta n/n \sim$ 20-30%,

which implies for an estimate of the peak electrostatic field amplitude, $\delta n/n \sim E^2/8\pi n_e T_e \sim 0.2\text{-}0.3$. This is close to the beam trapping estimate of $(W_p/n_e T_e) \sim 0.5$ for $(n_b/n_e) \sim 2 \times 10^{-3}$ and $E_b/T_e \sim 500$.

4.5.4.2 Relation to mm Wave Experiment

The ratio of the collisionless skin depth to the radius of the plasma-filled chamber is again much smaller than in Schumacher and Santoru's experiment, with $\delta_o/r_g \sim 0.03$ in this case: thus the plasma is essentially infinite. The beam energies are nonrelativistic, while those used in the mm wave experiment are nonrelativistic or only mildly relativistic.

It appears that this experiment can be in the strongly turbulent regime if the beam energy is high enough, so that the condition $(W_p/n_e T_e) > (k_{zo}\lambda_{De})^2$ is satisfied. Because the electron collision frequencies are less than the modulational instability growth rate, $\delta_{MOD} \sim \omega_{pi}(W_p/3n_e T_e)^{1/2} \sim 0.26\ \omega_{pi} \sim 10^7\ s^{-1}$, there doesn't appear to be quenching by collisions. As in Schumacher and Santoru's experiment, there is no radiation at ω_{pe}, which Michel et al. claim is due to the fact that the density gradients are too smooth.

There is no detectable radiation at $2\omega_{pe}$ from the mm wave experiment when there is only one beam present, as compared with this experiment in the strongly turbulent regime. One way to make a better connection between the experiment of Michel et al. and the mm wave experiment would be to arrange parameters so that the latter is in the strongly turbulent regime with only one beam present.

4.5.5 Experiment E

4.5.5.1 Summary of Experimental Results

In the experiment of Cheung et al., Ref. 65, the formation of density cavities, spikey turbulence, and electromagnetic radiation at ω_{pe}, $2\omega_{pe}$, and even $3\omega_{pe}$, were observed simultaneously when a cold electron beam was injected into an ambient plasma. The experiments were performed in a large, 1.8 m long, 1.8 m diameter, vacuum chamber. The argon gas afterglow plasma had typical parameters $T_e \sim 1.5$ eV, and $n_e \sim 2.3 \times 10^9$ cm. The experiment is basically steady state, with beam energy $E_b \sim 800$ eV, beam density $(n_b/n_e) \sim 0.2\text{-}4\%$. The

beam diameter is about 4 cm, so that the distance between the beam edge and the conducting wall is ~ 8 collisionless skin depths.

At high beam densities, e. g., $(n_b/n_e) \sim 2\%$, the wave intensity of the excited beam modes becomes strong enough to create density cavities in the region where it saturates. These cavities become of the order of $\delta n/n \sim$ 40-50%. As the density cavity deepens up to this value, the location of the peak in the EM emission shifts from ω_{pe} to $2\omega_{pe}$. The emission at $2\omega_{pe}$ is attributed to the process $\ell + \ell \rightarrow t(2\omega_{pe})$, in which two antiparallel propagating Langmuir waves trapped in a cavity coalesce to produce radiation at $2\omega_{pe}$. Since $(k_z\lambda_{De})^2 \sim T_e/E_b \sim 1.5/800 \sim 2 \times 10^{-3}$, and $(W_p/n_eT_e) > 0.2$, this experiment is in the strongly turbulent regime. (Not sure what the background pressure is, but because it's an argon afterglow plasma, it's probably low, and the electron collision frequency is probably lower than the modulational instability growth rate.)

4.5.5.2 Relation to mm Wave Experiment

The experiment of Cheung et al. is also a steady state experiment, with nonrelativistic beam energies. However, the ratio (n_b/n_e) goes to much higher values than has been used so far in the mm wave experiment, that is $(n_b/n_e) \sim$ 0.02 for the Cheung et al. experiment versus $(n_b/n_e) < 0.001$ for the mm wave experiment. If it's possible to go to larger beam currents, and therefore larger (n_b/n_e) in the mm wave experiment, then it may be possible to make connection with this experiment and observe $2\omega_{pe}$ radiation with only one beam present.

4.5.6 Experiment F

4.5.6.1 Summary of Experimental Results

The experiments of Kato et al., Ref. 66, involved the interaction of a relativistic electron beam with a plasma to produce high power (> 10 MW) broadband radiation. The experiment covered the range of beam to plasma density from $0.01 < (n_b/n_e) < 2$. They observed what appears to be a transition in the spectral behavior of the radiation, from weak turbulence, with most of the power emitted at ω_{pe}, to a regime at the highest values of (n_b/n_e), with

emission at frequencies $\omega >> \omega_{pe}$ and weak harmonic structure not predicted by soliton type emission theories.

The relativistic electron beam is pulsed, with a 50 ns FWHM, and it is high current ($I_b \sim 128$ kA), and annular ($r \sim 3$ cm, $\Delta r \sim 1$ cm), with an energy of $\gamma_b \sim 3$. The background plasma density is $n_e \sim 10^{13}$ cm^{-3}, so that the collisionless skin depth $\delta_o \sim 0.16$ cm, and there are many δ_os between the beam edge and the conducting walls of the chamber. The plasma is either unmagnetized or weakly magnetized.

There are some other experiments by these researchers in collaboration with other workers, referred to in Refs. 67 and 68, which are again interesting high power mw beam-plasma experiments. Reference 67 reports on the observation of both high frequency, $\omega \sim \bar{\omega}_{pe}$, as well as low frequency, $\omega < \bar{\omega}_{pe}$, radiation. The high frequency radiation resembles radiation from processes in type-III solar bursts: weak turbulence theory is used to explain the emission, even if the beam is stabilized by the modulational instability, because the damping of plasma waves by the radiation itself can prevent soliton collapse. The emission at low frequency was claimed to arise from scattering off density gradients near the wall of the plasma-filled chamber, where the density was lower.

Reference 68 reports on the observation of high power mw emission when a cylindrical drift tube chamber was modified to form a resonator for a relativistic electron beam-plasma system. The principal drift tube has a 10 cm radius, and the beam is annular, with a 2.5 cm radius. Various configurations, including screens mounted perpendicular to the beam at different distances, and additional coaxial drift tube structures, were investigated. The radiation peaks at the plasma frequency, but between the different configurations the peak power/Ghz, energy/Ghz, and bandwidth differed by an order of magnitude. This experiment was a longer timescale, $\tau \sim 15$ μs, lower current, $I_b \sim 12$ kA, and lower beam energy, $E_b \sim 500$ keV, experiment than the previous two. The beam propagates into a 20 cm diameter, 1.5 m long drift tube, with an axial magnetic field of a few kG. The background plasma density appears to be of the order of $n_e \sim 10^{12}$ cm^{-3}.

It was proposed by the authors that the results in Ref. 68 could be explained by a combination of two mechanisms: (1) radiation at ω_{pe} and $2\omega_{pe}$

from the plasma by strong turbulence, and (2) radiation by bunched electrons in the REB caused by electrostatic waves which act as a wiggler, with the emission double doppler shifted so that $\omega = \gamma_b^2 \omega_{pe}$. It's claimed that the reflected longitudinal plasma waves can provide a pump wave for the beam electrons, acting like a longitudinal "wiggler" with $k_z \sim \omega_p / v_b$.

4.5.6.2 Relation to mm Wave Experiment

These experiments are intense, relativistic beam experiments, unlike Schumacher and Santoru's experiment which is in the nonrelativistic to mildly relativistic regime, with low beam densities $(n_b/n_e) << 1$. If the mm wave experiment goes to larger beam currents and higher beam energies, then it may be possible to make more connection with these experiments. However, it might be interesting to do resonator experiments in the mm wave experiments, similar to Ref. 68. With appropriate beam and waveguide parameters, it would be interesting to see if radiation could result from a single beam, using various screen and drift tube structures.

5. REFERENCES

1. W. H. Bennett, Phys. Rev. 45, 890 (1934).
2. N. A. Krall and A. W. Trivelpiece, Principles of Plasma Physics (McGraw-Hill, p. 495, 1973).
3. R. N. Sudan, in Handbook of Plasma Physics, ed. by M. N. Rosenbluth and R. Z. Sagdeev; Volume 2: Basic Plasma Physics II, ed. by A. A. Galeev and R. N. Sudan (Elsevier Science Publishers, B. V. 1984).
4. A. A. Rukhadze and V. G. Rukhlin, Soviet Physics JETP 34, 93 (1972).
5. D. Hammer and N. Rostoker, Phys. Fluids 13, 1831 (1970).
6. R. B. Miller, An Introduction to the Physics of Intense Charged Particle Beams (Plenum Press, New York, 1982).
7. R. W. Schumacher and J. Santoru, "Millimeter-Wave Generation via Plasma Three-Wave Mixing", F49620-85-C-0059, Annual Report (April, 1986).
8. M. Mitchner and C. H. Kruger, Jr., Partially Ionized Gases (Wiley-Interscience, John Wiley & Sons, Inc., New York, 1973).
9. B. I. Aronov, A. A. Rukhadze, and M. E. Chogovadze, Soviet Physics-Technical Physics, 17, 877 (1972).
10. B. I. Aronov and A. A. Rukhadze, Soviet Physics - Technical Physics, 17, 1283 (1973).
11. B. I. Aronov, L. S. Bogdankevich, and A. A. Rukhadze, Plasma Physics, 18, 101 (1976).
12. A. B. Kitsenko and M. M. Shoucri, Plasma Physics 10, 23 (1968).
13. M. M. Shoucri and A. B. Kitsenko, Plasma Physics, 10, 699 (1968).
14. P. F. Ottinger and J. Guillory, Phys. Fluids 20, 1330 (1977).
15. P. F. Ottinger and J. Guillory, Phys. Fluids 22, 466 (1979).
16. P. F. Ottinger and J. Guillory, Phys. Fluids 22, 476 (1979).
17. T. Tajima, Phys. Fluids 22, 1157 (1979).
18. C. W. Roberson and K. W. Gentle, Phys. Fluids 14, 2462 (1971).
19. M. E. Jones, Phys. Fluids 27, 1928 (1983).
20. R. J. Briggs, in Advances in Plasma Physics, ed. by A. Simon and W. B. Thompson (Interscience, New York, 1971).
21. M. E. Jones, in the Conference Record of the 1982 IEEE Int'l Conf. on Plasma Science, Ottawa, Canada, May 1982, paper 1R8.
22. S. A. Self, M. M. Shoucri, and F. W. Crawford, Journal of Applied Physics 42, 704 (1971).

23. M. Seidl, W. Carr, D. Boyd, and R. Jones, Phys. Fluids 19, 78 (1976).
24. A. Bers, in Handbook of Plasma Physics, ed. by M. N. Rosenbluth and R. Z. Sagdeev, Volume I, Basic Plasma Physics I, ed. by A. A. Galeev and R. N. Sudan (North-Holland Publishing Co., 1983).
25. B. R. Kusse, M. S. Thesis, Dept. Electr. Eng., MIT, Cambridge, Mass. USA (1964).
26. A. Arapostathis, B. S. Thesis, Dept. Electr. Eng., MIT, Cambridge, Mass. USA (1976).
27. S. Cuperman, L. Gomberoff, and I. Roth, J. Plasma Physics 19, 1 (1978).
28. O. P. Gandhi, Microwave Engineering and Applications, Chapter 8 (Pergamon Press, New York, 1981).
29. W. E. Drummond, J. H. Malmberg, T. M. O'Neil, and J. R. Thompson, Phys. Fluids 13, 2422 (1970).
30. T. M. O'Neil, J. H. Winfrey, and J. H. Malmberg, Phys. Fluids 14, 1204 (1971).
31. S. Kainer, J. M. Dawson, and T. Coffey, Phys. Fluids 15, 2419 (1972).
32. W. Kruer, J. M. Dawson, and R. N. Sudan, Phys. Rev. Lett. 23, 838 (1969).
33. S. Hamasaki, private communication.
34. V. E. Zakharov, "Collapse and Self-Focusing of Langmuir Waves", in Handbook of Plasma Physics, ibid.
35. H. P. Freund, I. Haber, P. Palmadesso, and K. Papadopoulos, Phys. Fluids 23, 518 (1980).
36. K. Papadopoulos, Phys. Fluids 18, 1769 (1976).
37. K. Papadopoulos and H. P. Freund, Comments Plasma Phys. 5, 113 (1979).
38. V. N. Tsytovich, Physica 82C, 141 (1976).
39. A. A. Galeev, R. Z. Sagdeev, V. D. Shapiro, and V. I. Schevchenko, Sov. Phys. JETP 45, 266 (1977).
40. G. L. Payne, D. R. Nicholson, R. M. Downie, and J. P. Sheerin, J. Geophys. Research 89, 10921 (1984).
41. D. R. Nicholson, G. L. Payne, R. M. Downie, and J. P. Sheerin, Phys. Rev Lett. 52, 2152 (1984).
42. J. C. Weatherall, J. P. Sheerin, D. R. Nicholson, G. L. Payne, M. V. Goldman, and P. J. Hansen, J. Geophys. Research 87, 823 (1982).
43. D. R. Nicholson, M. V. Goldman, P. Hoyng, and J. C. Weatherall, Ap. J. 223, 605 (1978).

44. M. L. Goldstein, K. Papadopoulos, and R. A. Smith, "A Theory of Type III Radio Bursts", in Waves and Instabilities in Space Plasmas, ed. by P. J. Palmadesso and K. Papadopoulos (D. Reidel Publishing Co., 1979).
45. H. L. Rowland, Phys. Rev. Lett. 69, 1276 (1977).
46. S. Hamasaki, private communication.
47. Ya. B. Fainberg and V. D. Shapiro, Sov. Phys. - JETP 20, 937 (1965).
48. R. Lee and M. Lampe, Phys. Rev. Lett. 31, 1390 (1973).
49. D. Montgomery and C. S. Liu, Phys. Fluids 22, 866 (1979).
50. S. A. Kaplan and V. N. Tsytovich, Plasma Astrophysics (Pergamon Press, Oxford, 1973).
51. D. B. Melrose, Plasma Astrophysics, Volume 2 (Gordon and Breach Science Publishers, New York, 1980).
52. D. B. Melrose, Space Science Reviews 26, 3 (1980).
53. K. Kamilov, F. Kh. Khakimov, L. Stenflo, and V. N. Tsytovich, Physica Scripta 10, 191 (1974).
54. R. A. Smith, M. L. Goldstein, and K. Papadopoulos, Astrophys. J. 234, 348 (1979).
55. K. Papadopoulos and H. P. Freund, Geophys. Res. Lett. 5, 881 (1978).
56. M. V. Goldman, G. F. Reiter, and D. R. Nicholson, Phys. Fluids 23, 388 (1980).
57. B. Prasad, Phys. Fluids 19, 464 (1976).
58. G. Benford and D. F. Smith, Phys. Fluids 25, 1450 (1982).
59. D. A. Tidman and G. E. Weiss, Phys. Fluids 4, 703 (1961).
60. R. W. Schumacher, private communication.
61. T. Intrator, N. Hershkowitz, and C. Chan, Phys. Fluids 27, 527 (1984).
62. P. Leung, J. Santoru, A. Y. Wong, and P. Y. Cheung, in Physics of Auroral Arc Formation, ed. by S. I. Akasofu and J. R. Kan (American Geophysical Union, Washington, D.C., 1981).
63. I. Alexeff, J. Reece Roth, J. D. Birdwell, and R. Mallavarpu, Phys. Fluids 24, 1348 (1981).
64. J. A. Michel, P. J. Paris, M. Schneider, and M. Q. Tran, "Nonlinear Effects in a Beam Plasma System: Second Harmonic Emission and Density Depression Formation", presented at Aspengarden meeting (June 1982); M. Schneider and M. Q. Tran, Physics Letters 91A, 25 (1982).
65. P. Y. Cheung, A. Y. Wong, C. B. Darrow, and S. J. Qian, Phys. Rev. Lett. 48, 1348 (1982).

66. K. G. Kato, G. Benford, and D. Tzach, Phys. Fluids 26, 3636 (1983).

67. G. Benford, D. Tzach, K. Kato, and D. F. Smith, Phys. Rev. Lett. 45, 1182 (1980).

68. A. Ben-Amar Baranga, W. Main, G. Benford, and D. Tzach, Bull. Am. Phys. Soc.